Aus der Kinderklinik und Kinderpoliklinik im Dr. von Haunerschen Kinderspital,
Klinik der Ludwig-Maximilians-Universität München
Vorstand: Prof. Dr. Dr. Christoph Klein

UNTERSUCHUNG DER ENDOTHELIALEN GLYKOKALYX BEI FRÜHGEBORENEN DURCH MESSUNG DER PERFUSED BOUNDARY REGION (PBR)

EVALUATION OF THE ENDOTHELIAL GLYCOCALYX IN PREMATURE NEONATES BY MEASUREMENT OF THE PERFUSED BOUNDARY REGION (PBR)

Dissertation zum Erwerb des Doktorgrades der Medizin
an der Medizinischen Fakultät der
Ludwig-Maximilians-Universität zu München

vorgelegt von
Lea Rajwich

aus
München

Jahr
2021

Mit Genehmigung der Medizinischen Fakultät der

Ludwig- Maximilians-Universität zu München

Berichterstatter:	Prof. Dr. Orsolya Genzel-Boroviczény
Mitberichterstatter:	Prof. Dr. Andreas Holzinger

Mitbetreuung durch die promovierten Mitarbeiterinnen:

PD. Dr. Claudia Nußbaum

Dr. Alexandra Puchwein-Schwepcke

Dekan: Herr Prof. Dr. med. dent. Reinhard Hickel

Tag der mündlichen Prüfung: 15.04.2021

Table of Contents

1 Introduction

1.1 Blood Vessels: Focus on Capillaries

Blood vessels build a network that supplies every cell with oxygen and nutrition. A complex structured system is required to fulfill the task [1]. The system consists of arteries, capillaries, and veins in varying sizes and forms to optimize their various functions, and their different anatomic structures follow their different tasks. The main classification of blood vessels into arteries and veins is based on their task to deliver blood either from the heart to the periphery of the body or vice versa, whereas capillaries form the intersection of those two systems. Typically, the wall of arteries and veins consists of three layers: tunica intima, tunica media, and tunica externa [1]. The innermost layer, the tunica intima is built luminally of simple squamous endothelial cells (EC) covered by the glycocalyx and it is fixated on a basement membrane [2-4]. The internal elastic membrane separates the underlying subendothelial soft tissue from the tunica media [1, 5], which consists mainly of smooth muscle cells and to a smaller part of soft tissue. The tunica externa, attached by the external elastic membrane, consists of soft tissue that embeds nerves and sometimes vasa vasorum [1]. As form follows function, the microstructure of each part depends on the type of blood vessel, organ and task [1]. This general structure is different in the capillary system, which will be explained in detail below.

1.1.1 Anatomy

The anatomy of the capillary system must be viewed in context with its function [1]. The main purpose is to provide cells of the human body with oxygen transported by red blood cells and with plasma nutrients. A branched capillary mesh-work of 100 000 km total length is found in humans leading to a total surface of 2000 to 6000 m² resulting in a fitted diffusion area with an average distance of 50 to 80 µm from any cell to the capillary network [1, 6]. The partial share of the capillary network of each organ depends on the rate of its metabolism, i.e., the higher the metabolism of an organ, for example, liver and kidneys is, the denser is its capillary system [1, 6, 7].

A closer view of capillaries shows further function adapted characteristics. The size of a single capillary measures 1 mm in length and 5-10 µm in diameter, whereas the width of a passing erythrocyte is 7 to 8 µm [1, 6]. The capillary wall consists similar to the tunica intima of vessels of three layers: endothelial cells apically covered with a glycocalyx (GCX), pericytes (as soft tissue) and a covering basement membrane [8]. Cell adhesion molecules interconnect the endothelial cells, as well as an adapted number of tight junctions, that further regulate the intercellular passage of molecules [8]. Capillaries with continuous endothelium possess abundant tight junctions enabling only small molecules (4k Dalton) to traverse over the 10 to 15 nm thin clefts, in contrast to sinusoidal endothelium with loose intercellular connections that enables big molecules to diffuse from the blood into the tissue.

Sinusoidal endothelium is found, for example, in the liver. This organ's high intercellular diffusion is amplified by missing soft tissue and basement membranes. The intermediate type is the fenestrated one with continuous tight junctions, where diaphragm covered apical endothelial cell pores offer a fast direct diffusion through the endothelial cell, necessary in organs with high reabsorption and secretion, for example, the kidneys [1, 6-8].

The surrounding soft tissue, made up by pericytes, is in interdependence with the endothelial layer by nourishing and maintaining its function. As stabilizing supporting connective tissue, it is also crucial for newly formed capillaries in the process of vasculogenesis and angiogenesis [1, 9].

1.1.2 Physiology and Function

Mass transfer is the main function of capillaries [1, 7]. Every molecule that is transported from the blood to the tissue is either lipophilic or hydrophilic. Lipophilic agents possess physical-chemical characteristics that allow them to diffuse freely through endothelial cell membranes [1]. The transport of hydrophilic agents happens in three different ways to pass the blood vessel wall: diffusion, transcytosis, and carrier systems [8]. Usually, the kind of transportation depends on the agent's properties and organ's specific anatomy of the endothelial wall, as discussed in chapter *1.1.1. Anatomy* (p. 1) Diffusion occurs when the agent flows through intercellular clefts or the cell membrane [1, 7]. This process is mainly based on physical properties, i.e., it depends on differences in hydrostatic and colloid osmotic pressures, established by large proteins, between the blood vessel and the surrounding tissue as well as the concentration differences of the diffusing agent itself, and can be described with Starling's equation [6]:

"Net fluid flow = conductance * driving pressure, or

$$Q_f = K*(P_{mv}-P_{pmv}) - K_a*(\Pi_{mv}-\Pi_{pmv})$$"[10].

K is defined as the fluid filtration coefficient (based on surface area for filtration multiplied by hydraulic conductivity of the membrane) and K_a as weighted plasma reflection coefficient (regarding solutes passing the capillary membrane), P as hydrostatic pressure and Π as osmotic pressure in either the microvessel lumen (mv) or perivascular, for example interstitial space (pmv) [10-12]. Recently, the Starling equation had to be revised according to new insights about the endothelial glycocalyx [13] (see chapter *1.2.4 Function*, p. 11).

Free diffusion also depends on the close distance of capillary to the cell, which is around 50-80 µm [1, 7]. Diffusion is a fast and energy saving method to supply the tissue, so it contributes mostly to mass transportation [6]. It is directed from the blood to the surrounding tissue and vice versa, and its extent is adapted to the current demand. Properties of the capillary blood flow (velocity, pressure) are the most important influencing variables on tissue perfusion [1, 6, 7]. Slower and energy demanding is the transcellular transportation, which is used for molecules that are too big to enable free diffusion.

Specific carrier systems are available, or transcytosis occurs, when molecules are incorporated in plasmalemmal vesicles, both enable molecule passing through the endothelial cell itself [7, 8].

According to Starling, the hydrostatic pressure should be considered as an implying factor of capillary mass transfer. The hydrostatic pressure itself depends on many factors. Metarterioles, also called terminal arteries, give rise to capillary beds, reducing their diameter from 10 to 15 µm to 5 to 8 µm. Hydrostatic pressure decreases from 30 mmHg to 25 mmHg. The blood velocity in capillary beds is approximately 0.02 to 0.1 cm/s, that is required for blood/ tissue exchange and at the same time the pressure of the following venules is even lower, so continuous blood flow is guaranteed [6, 7]. The decreased blood flow velocity accounts for 80-fold faster diffusion speed compared to the blood flow, leading to a rapid blood/ tissue equilibrium [7].

The capillary pressure is maintained actively by the so-called precapillary sphincter, which is, in essence, the metarteriole's most distal encircling smooth muscle cell. Arteriolar constriction and dilatation are locally controlled by the concentration of nutrients and metabolites, but also by hormones such as norepinephrine. The precapillary sphincter can not only adapt to the local demand but also to variations in blood pressure as seen physiologically due to changes in cardiac output or pathophysiologically in hypo- and hypertensive states [7].

Besides blood flow behavior in the microcirculation in vivo that results from structure and properties of the microvessels (length, hematocrit, velocity), and the regulatory reactions of vessels to their local environment as described above, Pries et al. [14, 15] took also into account the rheologic phenomena of microvessel viscosity, such as the Fåhræus-Lindqvist effect and the phase separation effect. The rheologic phenomena are essential, as they minimize the growing resistance in small vessels by modulating the blood viscosity, as the blood resistance depends on the blood viscosity. The Fåhræus-Lindqvist effect explains minimal viscosity in blood vessels of 5 to 8 µm diameters due to the alignment of red blood cells (RBCs) in the center of the vessel (comparable to a single file movement) and hence decreasing cell/cell and cell/wall interactions. The phenomenon that hematocrit is reduced in the capillary beds to around 10 to 20 %, compared to approximately 40% in the rest of the cardiovascular system, can be secondly described by the phase separation effect. In short, this effect states that at branching sites of blood vessels, RBCs flow preferably to the bigger diverging vessel, so that the smaller vessel branch presents the mentioned decrease of RBC (hematocrit) [15]. Another variable that has to be taken into account in rheological considerations is the GCX further mentioned in chapter 1.2. *The Endothelial Glycocalyx (p. 5)*.

1.1.3 Development

The formation of capillaries starts in Carnegie stadium 8 (equivalent to an embryonic age of 21 to 24 days) with a cluster of mesodermal cells (hemangioblasts), extra-embryonal in the yolk sac and intra-embryonal in the lateral plate mesoderm's splanchnic layer. In the yolk sac, the central part of that

sampled hemangioblasts differentiates into hematocytoblasts (blood cells progenitor cells), whereas the circumferential cells become angioblasts (the later endothelial cells) [9, 16]. Within the embryo, the differentiating angioblasts begin to migrate to the developing organs where tube formation to immature vessels occurs [9, 16].

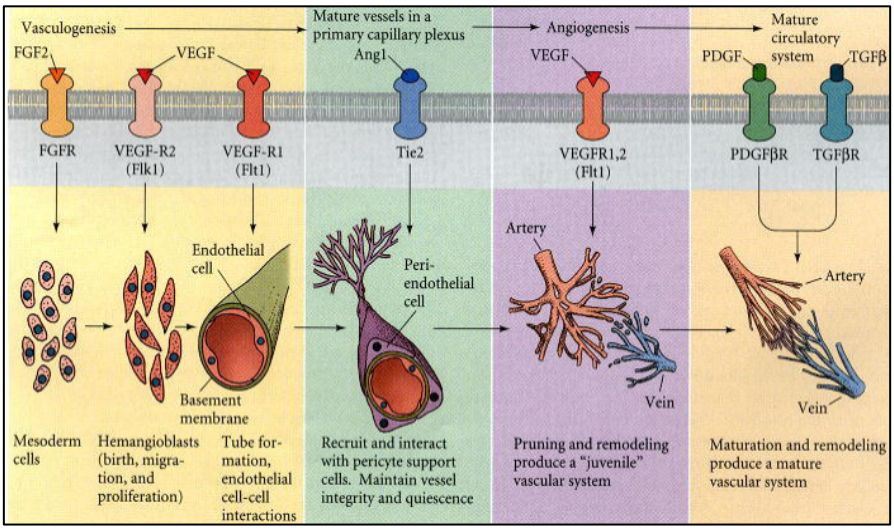

Figure 1: Schematic representation of vasculogenesis from premature vessel to unstable immature vessels, stable vessels and remodeled vasculature (9)

Under the further influence of paracrine factors, such as VEGF, the primary unstable vessels network matures into a branched stable constructed mesh-network (Figures 1 and 2) [16].

Another development may be seen in some parts of the arterial system. The arteries close to the heart do not develop from capillary plexus as described above, but from the aortic branches that descend in the pharyngeal arches [16].

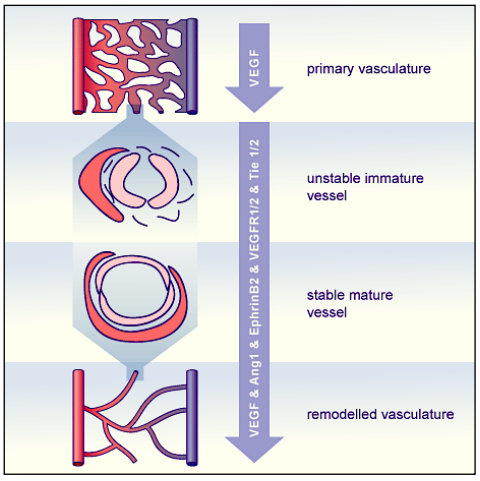

Figure 2: Simplified vasculogenesis (16)

Vasculogenesis is described as the development of blood vessels from single cells compounds (Figures 1 and 2) [9], whereas angiogenesis describes the development of new vessels departing from pre-existing ones (Figure 3) [17].

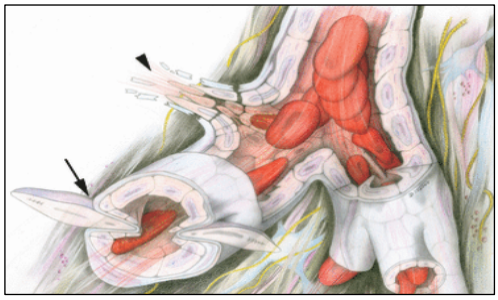

Figure 3: Sprouting angiogenesis' (arrowhead) and 'Non-sprouting angiogenesis' (intussusception) (arrow) (17)

1.2 The Endothelial Glycocalyx

1.2.1 Overview

The Glycocalyx (GCX) is anchored in the luminal surface of the endothelium as a network of proteoglycans (PG) plus linked glycosaminoglycans (GAG) and glycoproteins (GP), whereas the endothelial surface layer (ESL) is defined as GCX with attached plasma proteins and soluble glycosaminoglycans [18, 19]. This definition is theoretical, as the composition of all parts underlies a permanent change [18]. In this thesis, the term GCX embraces the considerations of ESL, except stated differently. Over the last couple of years, the GCX has become focus of interest in the research of vessel physiology and pathology. Nowadays, it is considered as one of the main etiological factors for vascular pathologies [13].

Before clinical thoughts have highlighted the role of the GCX, physiological research was done. The GCX gained interest, as the above mentioned rheologic effects (Fåhræus-Lindqvist and phase separation effect) explained only to some extent the in vivo measured lower hematocrit in capillaries [20]. Blood flow resistance in capillaries was higher than expected, up to 4 times higher than in glass tubes [21]. This may be explained by a decreased capillary diameter for the blood cell flow and increased blood viscosity due to the GCX [15, 20-22]. Capillary hematocrit values converged to expected values, when GCX was demolished [23]. The gained interest was the motivation for better visualization techniques, described in the next chapter.

1.2.2 History of visualization

The first attempts to visualize the GCX were made in 1966 by Luft et al. using transmission electron microscopy (TEM) that measured its thickness of only a couple of nanometers [24], and its role was diminished first. Theoretical calculations in a model hinted a bigger GCX, that could trap a slow flowing plasma layer of around 1.2 μm [20]. Assuming underestimation of the GCX dimension due to the damage caused by the fixation protocols used for electron microscopy [23, 25], better diagnostic techniques were necessary to get a more in-depth insight under physiologic conditions. One possibility to stabilize the GCX was directly infused new staining agents [26, 27]. Van den Berg, for example, used

Alcian blue 8GX in rat hearts and demonstrated that hypoxia had caused GCX degradation before fixation in previous studies [25].

Intravital studies of hamsters cremaster capillaries with bright-field and fluorescence microscopy by Vink and Duling were another turning point proving a thicker GCX layer of 0.4 to 0.5 μm [23]. The distribution of RBC columns was confined to the capillary center [23]. Here, the difference of anatomic capillary diameter from the functional capillary diameter of RBC was defined as erythrocyte-endothelial- cell (EEC) gap approaching the GCX thickness. Remarkably, the functional capillary diameter of RBC widened (the EEC gap shortened) after a transient white blood cell (WBC), which, due to WBC stiff structure, fully occupied the anatomical diameter thereby compressing the GCX (if the capillary diameter is below 10 μm). This change of RBC width before and after WBC passage was proportional to the directly measured EEC gap ("delta erythrocyte width/2 = 63% EEC gap") [23]. That approach based on the capability of RBC to adjust their form to capillaries in contrary to WBC was the foundation for orthogonal polarization spectroscopy (OPS)-Imaging. Especially as in human studies direct measurement of anatomical diameter was not possible as endothelial cells lack hemoglobin and hence could not be visualized similarly. Calculating the differences of RBC columns before and after passing WBC (= ΔRBC column/2) in a short video, is used for the approximation of the GCX dimension [28]. In hamster capillaries, the mentioned proved gold standard [23], the direct intravital measured gap of erythrocytes to endothelial cells (EEC) was proportional to OPS acquired values, as mentioned underestimating the intravital EEC gap in relation to its size by roughly 37% [28]. Additionally, in the non-invasive clinical setting in humans, OPS measured sublingual capillaries GCX correlated with the systemic volume of the GCX. The systemic GCX volume has been measured as the difference of circulating plasma volume (calculated for example, by fluorescent labeled RBC and sampled hematocrit) to total intravascular volume (dilution of GCX permeable tracer, for example, dextran 40) [28] and proven to be a reliable value [13]. OPS gained values were reproducible [28].

Sidestream Dark Field (SDF) imaging, the succeeding technique, is relying on similar video visualization [29, 30]. As that method was used for our study, SDF imaging is to be discussed in detail in chapter 2.5.2 *Sidestream Dark Field imaging* (p. 20). The main disadvantages of OPS and SDF imaging were, besides estimating the GCX based on its compressible part, the restriction to superficial vessels. Recently, it was also possible to visualize the GCX in animal studies or in vitro by labeling it with fluorescent GCX specific antibodies. The labeled GCX is either visualized by fluorescence microscopy or by confocal laser scanning microscopy (CLSM) [31]. The scattering effects for deeper lying vessels are reduced in two-photon LSM (TPLSM) [18, 32]. The visualization methods, mentioned above, measured different GCX sizes, but when comparing different methods, the species and the kind of vessel should be also considered (see Chart 1).

	Method	Vessel	GCX thickness (µm)
Luft et al. [24]	TEM + ruthenium red	Capillaries	0.02
Van den Berg et al. [25]	TEM + Alcian blue 8GX	Rat myocardial capillaries	0.20 - 0.50
Haraldsson and Rostgaard Qvortrup et al. [26, 27]	TEM + fluorocarbon	Rat glomerular capillaries Rat intestinal fenestrated capillaries	0.06 - 0.20 0.05 - 0.10
Vink et al. [23]	OPS	Hamster cremaster capillaries	0.40 - 0.50
Shore et al. [31]	CLSM	Human umbilical vein	2.50 ± 0.10
Megens et al. [32]	TPLSM	Mouse carotid artery	4.50 ± 0.10

CHART 1: GCX THICKNESS IN COMPARISON TO VISUALIZATION METHOD AND VESSEL TYPE

1.2.3 Structure and composition

Another aspect, when discussing varying GCX sizes, is its continuous remodeling. The changes make it rather difficult to provide a static picture of the layer, as shown in Figure 4, with membrane-bound proteoglycans linked to glycosaminoglycans and glycoproteins [18]. Considerations about the continuous remodeling inlcude rheological and enzymatic influences.

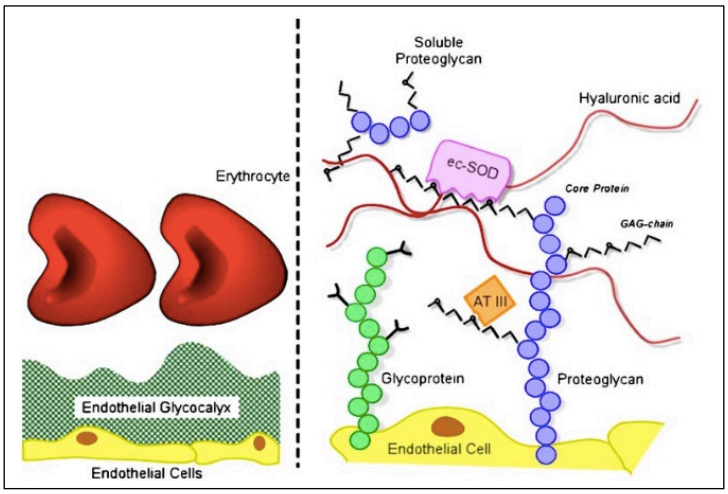

Figure 4: Non-scaled representation of the GCX "Left: …GCX as a cell exclusion zone, located on the luminal side of the vascular endothelium…Right: ... proteoglycans, with long unbranched glycosaminoglycan side-chains (GAG-chain) and glycoproteins, with short branched carbohydrate side-chains. Incorporated ... are plasma and endothelium derived soluble components..." (18)

Proteoglycans/ Glycosaminoglycans

An additional description of proteoglycans is based on the research results of Cruz-Chu et al., who used an experimental simulation (an all-atom-molecular-dynamics simulation) to provide an extensive but slightly modified and simplified picture of the GCX in vitro [19]. Overall, proteoglycans consist of a protein (so called core protein), which is glycosylated by covalently bound GAG chains [33]. Core proteins are either anchored to the membrane (syndecans and glypicans) or are plasma soluble and secreted as unbound PG (versican, decortin, mimecan, perlecan and biglycan) at the end of synthesis [19].

Various kinds of syndecans have been linked to specific tissues and tasks due to the influence of chemokines in the PG synthesis [18]. The structure of syndecans is here described on the basis of Syndecan-4, which is not tissue specific. It consists of the α-helix dimer with a cytoplasmic (connected to actin filaments within the cell), a transmembrane (anchors the whole core protein) and an extracellular (bound to a variant amount to GAG) domain. Due to the structure, the PG is capable of transferring an external impulse to the inside of the cell (transduction). Glypican shows another anchoring pattern by a glycosylphosphatidyl (GPI-) anchor [19].

At the beginning of PG biosynthesis, the core protein is ribosomally translated. After translation of the core protein, PG is linked to GAG in the endoplasmic reticulum (ER) and Golgi- apparatus. In detail: SER-β3-Xyl-β4-Gal-β3-Gal-β3-GlcUA- (simplified in Figure 5) [18, 33].

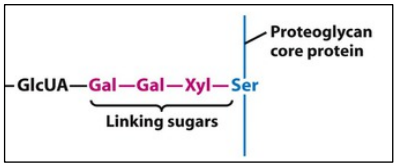

Figure 5: Simplified PG structure. Ser: serine, Xyl: xylose, Gal: galactose, GlcUA: glucuronic acid (33)

More sugar acids or hexosamines (N-Acetyl-Amino sugars) are added on the glucuronic acid to synthesize the complete GAG. The differences of the several kinds of GAG are based on "their monomer composition, by the position and configuration of their glycosidic linkages, and by the amount and location of their sulfate substituents". Hyaluronan is the only non-sulfated GAG [34]. The GCX consists mostly of heparane sulfate (HS) (50 to90%) and chondroitin sulfate (CS, 10 to 20%), which normally appear in a ratio of 4:1, as well as hyaluronic acid (HA) and keratan sulfate (KS).

The properties of GAG cause different biochemical and physical effects. The GCX is negatively charged due to the anionic oligosaccharides and sulfates. For example, HS is not folded in solution, so that the influence of electrostatic interactions becomes more relevant, and elongation increases the electric charge [19]. Almost all GAGs are connected to a proteoglycan (PG). HA is the only exception because it is not bound to any core molecule, but it is attached to the CD 44 receptor of endothelial cells [18].

Glycoproteins

Glycoproteins (GP) are among the main groups that are involved in the synthesis of GCX [18, 35, 36]. The common property of GP are their short and branched chains of 2 to 15 oligosaccharides [35, 37]. These GP are either found within endothelial cell adhesions molecules (for example, integrins, selectins and members of the immunoglobulin superfamily described in Chart 2) or as factors of coagulation and fibrinolytic cascades [35, 36, 38].

Depending on their task, GP are also synthesized within the EC continuously and/ or they underlie inflammatory stimuli [39]. Part of the pro-inflammatory cell adhesion molecules are retained by the lipid bilayer of the endothelial cell and are covered in a non-inflammatory state by the GCX. Under

inflammatory conditions, pro-inflammatory PG are uncovered. Selectins induce a response in WBC trafficking with initiating the WBC/ EC binding while integrins strengthen it [40, 41]. Likewise, in hemostasis the GP Ib-IX–V complex plays a key role because it can bind von Willebrand factor or P-selectin and thus recruit platelets to the endothelium [42]. Some known functions are illustrated in Chart 2.

GP Subgroup	**Structure**	**Examples**	**Function**
Integrins	αβ heterodimer with one out of 18 different α- and 8 different β-subunits [43]	8 different forms on EC: α1β1, α2β1, α3β1, α6β1, α6β4, α5β1, αvβ3 and αvβ5	connecting to extracellular matrix molecules (ECM), for example laminin, fibronectin and collagen - receptor configuration induces intracellular response in form of cell adhesion, proliferation and differentiation, angiogenesis and stabilization in the basement membrane [43, 44]
Selectins	Cytoplasmic, transmembrane and luminal part, which has a lectin and EGFR site [18, 45]	P- and E-Selectin	triggering inflammation by recruiting and binding WBC through slower rolling on ECs [45-47] - E-selectin: de novo synthesis (delayed answer), influenced by cytokines (IL-1, TNF-α and LPS) [48] - P- selectin: stored in Weibel-Palade bodies within ECs and translocated by thrombin and histamine [48]
IG Superfamily (CAM= cell adhesion molecules)	transmembrane molecule with an immunoglobulin-like luminal end [17]	platelet/endothelial cell adhesion molecule 1 (PECAM-1)	binding sites for leukocytes (extravasation) and platelets, forming EC/EC junctions [49]
		vascular cell adhesion molecule 1 (VCAM-1)	binding sites for leukocytes (adhesion and extravasation) and platelets (clotting) [50]
		intercellular adhesion molecule 1 (ICAM-1)	binding sites for leukocytes adhesion and extravasation) and platelets [17]
		intercellular adhesion molecule 2 (ICAM-2)	WBC trafficking, angiogenesis [49]

CHART 2: GLYCOPROTEIN ADHESION MOLECULES

Plasma Proteins

Abundant molecules, especially proteins and soluble PG, derived from either the blood or the endothelial cells, have been found to bind to the GAGs within the GCX, thereby contributing to its

organization and charge [18]. These plasma proteins and the GCX build together to form the whole endothelial surface layer (ESL) [36].

Cruz-Chu et al., for example, studied the binding of FGF-2 to HS. In their simulation they were able to illustrate the binding process and that strongly negatively charged areas attract several FGFs that oligomerize, which is essential to activate the receptor [19]. Furthermore, the study indicated, that many factors of the coagulation system were attached to the GCX, for example, antithrombin III or thrombin. The lipoprotein-protease and its substrate LDL were also attached [19].

Role of Shear Stress and Enzymatic Influence

The boundary region of the flowing blood and the GCX/ endothelium is a complex physical mechanical system. Blood is a not-Newtonian fluid and blood vessels are not rigid tubes but are branched and vary in size. In general, two main forces of blood flow stress the boundary region and EC. The pulsatile blood pressure forces the compression of GCX/endothelial wall. The shear stress works parallel to the blood flow and it causes frictional force [51]. The GCX functions as barrier coat and the shear stress on ECs is diminished. The mechanical forces are transduced via the GCX into ECs directly by conformation changes of the luminal-exposed endothelial receptors [51, 52]: Shear stress induces shedding or degradation of GCX components such as GAG chains, for example, HS [53], and an increase in shear stress results in a conformation change of HS- chains and syndecan molecules [19]. The conformation changes are transduced to the inner of the cell [19]. Those changes due to shear stress could result in NO induced vasodilation [36], but the specific degradation of HS results in significantly lower induced NO vasodilation [54, 55].

In Figure 6, Weinbaum et al. presented an example of intracellular transmitted shear stress, called the “bumper car”– model, where the cytoskeleton was re-organized and cell body changed its confirmation to adjust to the increased shear stress [36]. Figure 6 indicates that when GCX is intact, shear stress is transduced by core proteins to the underlying cytoskeleton including stress filaments, DAPB (dense peripheral actin band), integrins and gap junctions. Those changes loosen intercellular bonds, while the basal bonds within the basal lamina stay intact. Like rubber bumps, the flexibility of the cell membrane protects adhesions on the basal lamina, whereas when the GCX is compromised, ECs transmit the induced stress directly on to the basal connection [36, 52, 56].

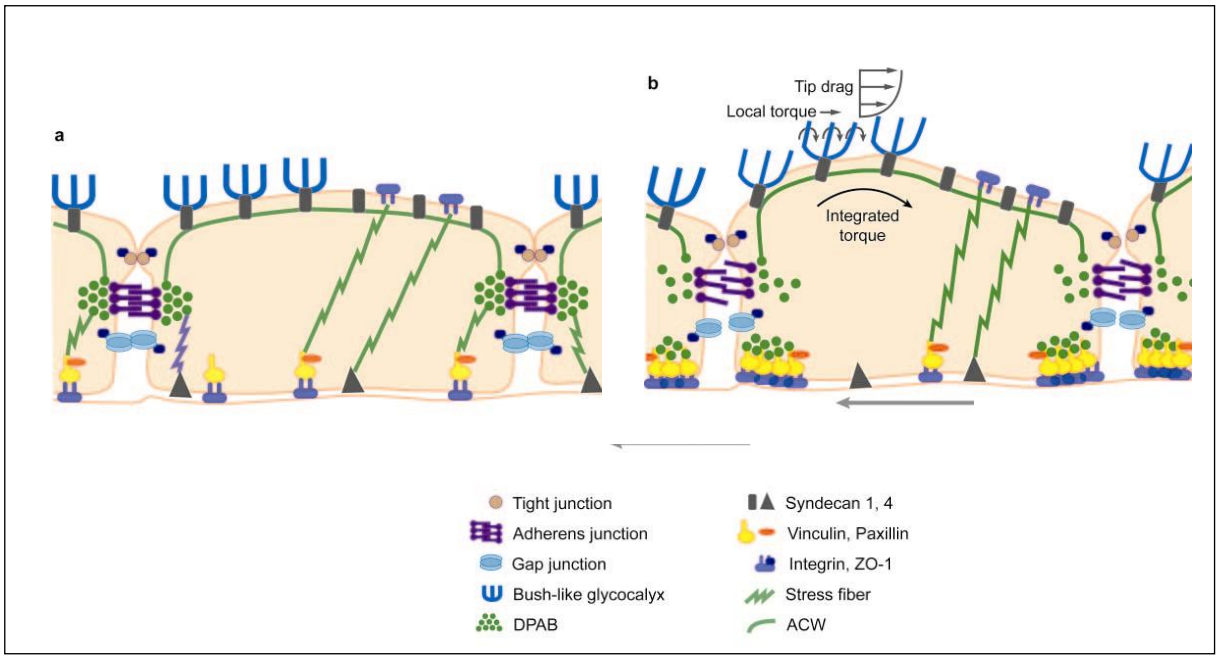

Figure 6: "Sketch of the conceptual "bumper-car" model for the structural organization of the EC in response to fluid shear stress" a, steady state without shear stress. b, shear stress is transduced to the cytoskeleton leading to shear stress adapted intercellular adhesions (36, 52)

Weinbaum et al. state that despite shear stress induced NO, the release depends on various mechano-sensors and endothelium with a degraded GCX still reacts to shear stress [36].

In vivo, analog enzyme induced shedding has been observed in critically ill patients with higher blood levels of HS and other linked components of the core protein syndecan-1 [57]. In a non-inflammatory state, the shedding occurs physiologically in a small amount of GCX bound matrix metalloproteases or heparinase and is accelerated in inflammation by binding receptors, co-enzymes, and cytokines like TNF-α [58-60].

1.2.4 Function

Functions of GCX are best evaluated based on its fragile structure, and any form of degradation leads to endothelial dysfunction, a vicious circle [13, 18]. As the boundary region, the negatively charged mesh of GCX is responsible for an intact barrier that mediates the interaction of blood and tissue [8].

When ubiquitous similar intravascular and interstitial osmotic pressures were detected, Starling's equation was revised [13]. Regarding the difference of osmotic pressure as one of the leading forces counteracting hydrostatic pressure, retaining the fluid inside the vessel was insufficiently explained [61, 62]. New insights of the GCX were included for a further validation of Starling's equation. First, the difference of osmotic pressure does not exist between the ECM and the blood vessel. However, a difference in osmotic pressure between the luminal (protein- rich) and the endothelial (protein- poor) layer of the GCX as presented by the Michel-Weinberg model in Figure 7 was detected [36, 62].

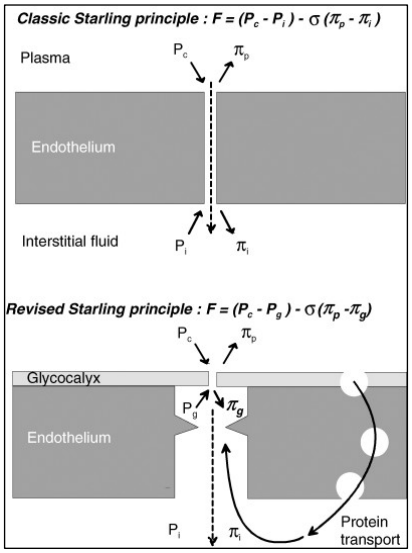

Figure 7: Classic vs. revised Starling principle. "Changing nature of Starling principle for fluid exchange across non-fenestrated endothelium. F, sum of 'forces' acting across semipermeable membrane…. Continuous short arrows denote force directions; denote flow" (σ= reflection coefficient; simplified by leaving out K, the fluid filtration coefficient. Other symbols as explained in chapter 1.1.2., physiology and function) (62).

Second, the negatively charged GCX hinders big proteins from crossing the boundary blood/ EC region. This effect can be maximized by binding HES (hydroxyethyl starch) or albumin, which decreases the hydraulic conductance (see chapter 1.1.2 *Physiology and Function,* p. 2). The binding likely tightens the diameter of transmembrane pore channels leading to less extravasation of small proteins (roughly 40 kDalton) [63, 64]. Hence, the GCX is the main structure to retain fluid in vessels. Thus, fluid shifts in ischemic or critical illness and vascular pathologies were highlighted as a sequela of a damaged, thinned GCX. GCX damages either result from a general breakdown, a change of its GAG composition and/ or modification and can lead to a pro-pathological state and its consequential effects [13, 18].
Not only are albumin and HES are incorporated, but cytokines, ligands to EC receptors, WBC and more are harbored in the GCX [36]. Interaction of cell-/ or blood-derived factors with EC, vascular tone, blood rheology, and permeability of blood vessels belong to the so far recognized GCX functions. Examples of the cell/ endothelium interaction were already given in chapter *Glycoproteins* (p. 8), as well as of the influence on the vascular tone in chapter Role of *Shear Stress and Enzymatic Influence* (p. 10), and the rheologic influence in chapter 1.1.2. *Physiology and Function* (p. 2). An insight into the different underlying pathologies and their sequelae are highlighted below.

1.2.5 Pathology

GCX alterations and succeeding endothelial dysfunction are increasingly considered to be crucial in the pathophysiology of various diseases and their progression. Simplified, at the beginning of endothelial dysfunction, disruption of GCX promotes the recruitment of WBC and platelets, producing oxidative stress (reactive oxidative species, ROS) and proteases. This reinforces GCX degradation, which leads to

further impairment of its functions to maintain the blood/ vessel/ tissue equilibrium [13, 18, 65]. Endothelial dysfunction is known to promote vascular pathologies in the following affections.

Diabetes Mellitus

Diabetes mellitus (DM) is a disease with several vascular pathologies [53, 66-68]. Stressing the role of GCX alterations and succeeding endothelial dysfunction, high sugar levels are supposed to contribute to the shedding of the GCX. In DM patients, high plasma levels of HA and hyaluronidase as tracers for GCX degradation were measured [53, 66-68]. In addition, a thinned GCX could be observed following a controlled state of hyperglycemia [68], as well as in patients with DM type 1, where the findings were especially pronounced when the patients suffered concomitantly from microalbuminuria, a common side effect of DM [66].

Atherosclerosis

Atherosclerosis is thought to arise from a damaged GCX [69-71]. High LDL cholesterol levels are proven atherogenic risk factors [69]. By inducing high levels of LDL, the GCX thickness was significantly reduced. The effect could be weakened by adding SOD and catalase, as the LDL levels decreased [70]. Underlining these results, regions of the carotid artery with a high prevalence of atherosclerosis showed a reduced GCX, stressing the likely involvement of GCX damage in the disease development [71].

Hypertension is another atherogenic risk factor that releases ROS damaging the GCX [72]. In retinal and choroid vessels, hypertension triggered alone and amplified the DM mediated endothelial dysfunction [65].

Ischemia/ Reperfusion

Partial or total ischemia and consecutive reperfusion also promote shedding of the GCX [55, 58]. For many years cytotoxins (mainly free radicals and lipid mediators) have been investigated mediating cell responses of inflammatory cells (mast cells, leukocytes) that causes ECs to swell and even to detach from their basement membrane [72].

Nowadays, the focus shifted on their effect on GCX and endothelial dysfunction as the crucial step in ischemia-induced damages. Free radicals and lipid mediators were ascertained to result in GCX shedding by detection of increased levels of GCX derived GAG in blood plasma. This hypothesis was further supported as reducing the synthesis of radicals by inhibiting producing enzymes such as xanthine oxidoreductase or by administering pertussis toxin to inhibit G-protein coupled enzymes, resulted in decreased shedding [55, 58].

Inflammation and Sepsis

Similarly, inflammation causes a similar cascade as seen in ischemia/ reperfusion, even though the triggers differ [13, 18, 73]. As an example, TNF-α is an acknowledged inflammatory protein [74] that leads to GCX shedding [73]. Henry and Duling proofed GCX shedding occurred after infusion of TNF-α in cremaster microvessels and is amplified when WBC adhesion is not prevented for example, by blocking selectins (Figure 8) [73].

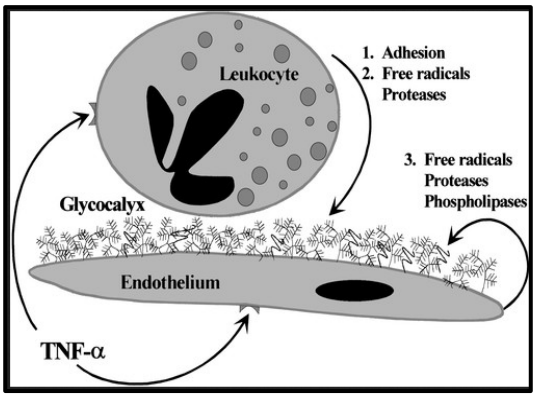

Figure 8: Shedding of GCX by TNF-α (via WBC, GCX or EC derived degrading enzymes) (73)

The influence of TNF-α on WBC/ GCX is based on an increased cell adhesion due to GCX shedding and hence endothelial exposure of E-selectin, emphasized by LPS administration [13, 18]. Additionally, applying TNF-α showed recruiting and attaching white blood cells by uncovering VCAM-1 and ICAM-1 as well as an increase of vascular permeability [73]. Secondly, edema formation is observed, as after GCX shedding albumin is no longer linked to the GCX and blood components are not retained in vessels, so albumin movement through endothelium is eased (compare chapter *1.2.4. Function*, p. 11) [25, 75]. Commonly known, inflammation supports a pro-coagulatory state, which Spaan et al. could explain by an inverse correlation between the GCX thickness and the pro-coagulation tendency likely due to PECAM exposure [70].

This insight might also be important for the clinical evaluation of critically ill patients in the future, as a higher GCX damage resulted in higher complication and mortality rates [76].

1.2.6 Development

The GCX that regulates vasculo- and angiogenesis plays a key role in pathologies and physiological development [77]. Henderson-Toth et al. focused on the role of the GCX during embryogenesis in quails [77]. Initially, they showed that the GCX is present from the 14-somite stage on, which is the same time point the blood flow starts. At that time, GCX presented immaturely with many luminal protrusions and immature ECs. Maturation was impaired by specific degradation of GAGs. That every GAG has a different task based on its composition was already mentioned before (chapter *Proteoglycans,* p. 7*/ Glycosaminoglycans,* p. 8), but now, it could be shown that the main GAGs also play an important role in vasculogenesis [77].

Next to the above-described GCX- mediated transduction between blood and ECs (chapter 1.2.4 *Function*, p. 11), GAGs facilitate gene expression essential for vascular development, either adapted to shear stress or directly stimulated by receptors ligands. As an example, HS functions as the endothelial cell binding site for FGF-2, activating a signal cascade for ECs to mature and develop a polar structure [77, 78]. Through shear-stress, signal cascades with influence on gene expression (for example, of ephrinB2 and neuropilin1) are modulated, necessary for the arteriovenous maturation, which explains why blood flow is crucial for the maturation of blood vessels [79, 80].

As stated above, hyperglycemia in DM has a negative effect on the GCX. Reviewing the correlation also in embryology, Henderson-Toth et al. combined their findings with those of Madri et al., who showed that maternal DM impairs the fetal expression of VEGF-a and platelet-derived endothelial growth factor (PDGF) causing vascular abnormalities. VEGF and PGDF expression were both impaired by GAG degradation (either by hyaluronidase or high sugar levels) so that a possible shared pathologic pattern with focus on the GCX could be postulated [77, 79].

1.3 Prematurity

1.3.1 Definition

Prematurity is defined as birth before 37 completed weeks of gestation [81]. Every year around 15 million newborns are born prematurely globally, making in 2014 10.6% of all births [82]. A sub-classification into three groups based on the gestational age at birth (in weeks [w]/ days [d]) is common: extreme preterm (born before 28w + 0d), very preterm (28w till 31w + 6d) and moderate to late preterm (32w till 36w + 6d) [81]. 2013 prematurity was the second most common reason for mortality under the age of 5 years (29%) [81]. These numbers demonstrate the importance of dealing with prematurity, asking for improved prevention and better treatment of prematurity's consequences.

1.3.2 Complications of prematurity with focus on vascular pathologies

When discussing the complications, meaning mortality and short- and long-term co-morbidity of prematurity, it is rather challenging to classify the direct sequelae only based on prematurity. In general, the earlier a preterm infant is born, the more vulnerable it is. There are diseases, that can almost only be seen in preterm newborns, for example, necrotizing enterocolitis (NEC) or bronchopulmonary dysplasia (BPD), but on the other hand, common neonatal diseases also occur, partly with a higher than average incidence such as infections [82-84].

As this study investigates the GCX in preterm infants, the already established relations between prematurity and microvascular pathologies are mainly of interest. An altered microcirculation and endothelial function have been observed in adolescents born preterm [85]. Their altered microcirculation with higher functional vessel density (FVD, an perfusion marker) of cutaneous vessels

compared to mature neonates is a finding that persists from the perinatal period to adolescence [85, 86]. Adolescents born preterm show an increased risk for atherosclerosis illustrated by an increased intima thickness of the carotid artery (cIMT), an early indicator for atherosclerosis [85]. The population of prematurely born adults features atherogenic risk factors such as higher systolic blood pressure, heart rate and hypertension [87]. Those features were shown to impair the GCX contributing to atherosclerosis in the carotid artery (chapter 1.2.5 *Pathology,* p. 12) [71]. It is state of research to find out if the altered microcirculation in prematurely born adolescents/ adults is the reason for their described increased atherogenic risk factors and the succeeding arteriosclerosis.

Besides the sequelae of prematurity, monitoring microcirculation in preterm neonates has been investigated increasingly in the last years [88, 89]. Generally, perfusion can well be evaluated by microcirculatory assessment, for example in anemic preterm neonates: microcirculatory assessment pictured even more sensitively than usual clinical assessment the cardiovascular reaction after blood transfusion [88]. In septic preterm neonates microcirculatory perfusion is reduced [89]. Anemia, as well as sepsis, are two pathologies with high indices in prematurity that have to be detected fast for immediate consequences [88, 89].

The persistent ductus arteriosus is especially interesting in regard to GCX function. Physiologically, due to higher oxygen saturation and altered cytokine levels, the vascular muscle of the ductus arteriosus constricts shortly after birth. Small vessel injuries analog to atherosclerosis occur, leading to annealing of thrombocytes [90, 91]. In prematurity, the duct often persists open [91]. One reason is the immature platelets in neonates (their maturation is proportional to gestational age), and instable thrombus formation probably due to immature adhesion molecules (for example, the above mentioned ICAM ligands) [92]. Till now, it can only be assumed if GCX dysfunction in prematurity contributes to that described endothelial/ thrombocyte dysfunction.

Retinopathy of prematurity (ROP) is another example of the high susceptibility of vascular development in prematurely born neonates. In preterm neonates, retinal vascularization is not completed. The premature retinal vessels are susceptible to disruptions of their normal maturation, caused by non-physiological pO_2 levels leading to relative retinal hyperoxia (phase one of the two-phase model of ROP development). In the second phase, the increased metabolic demand of the photoreceptors cannot be met by the incompletely vascularized retina. Under hypoxia, photoreceptors release large amounts of VEGF resulting in disordered unstable vascular proliferation [93]. As pointed out above (chapter *1.2.6 Development,* p. 14), VEGF function is GCX modulated [77]. High glucose levels amplify the development of ROP [94]. In the section on vascular consequences of diabetes mellitus (chapter 1.2.5./ *Diabetes mellitus in Pathology,* p. 13), high blood glucose levels were shown to induce shedding of the GCX, hinting towards a possible involvement of the GCX in ROP as VEGF alterations through hyperglycemia are known [79].

1.4 Aim of The Study

The aim of the study was to approach the development of the perinatal GCX. The interface of GCX in vascular development can be assumed to play a role in prematurity related vascular pathophysiology. The role of GCX in prematurity is a new field of research with increasing importance, and this work is focused on several related questions, assessing the GCX by the endothelial perfused boundary region (PBR):

- Can measurements of the perfused boundary region (PBR), indicating GCX, be used in preterm neonates?
- Are values of the perfused boundary region (PBR) related to clinical or laboratory parameters?
- How thick is the perfused boundary region (PBR) in preterm neonates shortly after birth?
- Does the perfused boundary region (PBR) depend on gestational age (GA), as indicator of the neonate's maturity at birth?
- Does the perfused boundary region (PBR) depend on postnatal age?
- Can the extrauterine development of the perfused boundary region (PBR) be compared to the intrauterine one?

2 MATERIAL AND METHODS

2.1 Study design

A single-center prospective observational study with a weekly follow up was designed to evaluate changes of the GCX over time. Precisely, PBR was used as an indirect GCX surrogate. In every assessment short video sequences to calculate PBR were obtained non-invasively at the helix of one participant's ear using a Sidestream Dark Field (SDF) imaging camera. Clinical parameters were recorded at the time of the measurement. SDF measurements were conducted, whenever possible, parallel to clinically indicated blood draws, gaining additionally capillary or venous blood gas analyses for the study. When a more extensive blood sample was obtained, further blood results, e.g. infectious parameters, were also recorded.

The study group was divided into neonates born very premature before the completed 30th gestational week (≤ 29w + 6d; n = 20) vs. neonates born moderately premature afterwards up to the completed 37th gestational week (30w + 0d till 36w + 6d; n = 19) to search for differences in the GCX thickness at birth and during maturation. A parallel study with term babies served as control group.

The ethics committee of the medical faculty of the Ludwig-Maximilians-University in Munich, Germany approved the study design before the study started. Before a child was included in the study, the informed consent of the parents was obtained. The parents of preterm babies were briefed extensively about the study, after which a detailed information letter was handed out. The parents were given at least 24 hours to consider, during which they could ask further questions. Furthermore, the parents were given the opportunity to be present at all assessments. If the parents agreed to the participation of their child, written informed consent was obtained. Nevertheless, the parents could recall their consent at any time, which happened once for personal reasons.

2.1.1 Patients

Recruitment/ Inclusion and exclusion criteria

The study started in December 2013 and all preterm babies born at the “Klinik und Poliklinik für Frauenheilkunde und Geburtshilfe, Campus Innenstadt” of the Ludwig-Maximilians-University Munich, were screened for possible study participation. Until the end of 2014, 39 patients were included.

Clinically unstable neonates were excluded. Other exclusion criteria were morphologic variations, such as ear malformations (no such malformations occurred during the time of the study), suspected syndromes or pigmented skin due to possible technical limitations of the SDF imaging recordings.

2.2 Measurement schedule

The longitudinal design involved weekly examinations. The first measurement was scheduled at the time of the newborn screening, about 36 to 72 hours after birth. The second measurement was done between the 5th and 7th day of life. Further measurements were planned in a weekly following schedule: NS = newborn screening, 1st week of life (5th to 7th day), 2nd (8th to 14th day), ..., 13th week (85th to 91st day). The end point was set at the gestational age of 39 weeks or discharge from the hospital, resulting in a maximum of 14 measurement time points. Each measurement was performed within a time frame of 12 hours before or after taking a blood sample. Since taking a blood sample is a medical intervention that causes pain, the needed blood gas sample was only acquired if taking a blood sample was medically justified. That requirement for blood samples was a limiting factor. Due to this restriction and the aim to obtain a relevant number of measurements, evaluations were carried out in a weekly interval of 5 to 9 days (regular measurement time point ± 48 hours).

2.3 Laboratory Data

A capillary or venous blood gas sample was drawn to gain further information on the preterm newborn's medical condition, and to check for possible correlations with the microcirculatory measurement results. pH, pCO2, pO2, base excess (BE) and HCO3- were normally drawn for evaluation of the acid-base homeostasis with a capillary blood gas. When those parameters were insufficient for medical reasons, venous blood samples were drawn. Hemoglobin (Hb) and hematocrit (Hct), bilirubin, glucose and lactate were recorded, as well as when the infant was tested for CRP or IL-6 to detect infections.

2.4 Clinical Data

Besides weight and age, vital parameters were recorded at each time point, including blood pressure (mean arterial pressure= MAP), oxygen saturation (SpO2), heart rate (HR), perfusion index (PI) and respiratory rate (RR).

During the first measurement, birth-related data including the APGAR score were recorded.

2.5 Microcirculatory Data Collection

2.5.1 Overview

PBR, an inverse surrogate gauge for endothelial GCX, was measured non-invasively using a SDF camera to visualize the microcirculation. The camera covered with a sterile cap was put with very light pressure and a drop of saline on the infants (either right or left) antihelix. Since only small movements could be tolerated, this was mostly done while the infants were sleeping. A simplified overview of acquiring the GCX measurements can be described as the following. The SDF camera produced a picture of the perfused cutaneous vessel network (Figure 9):

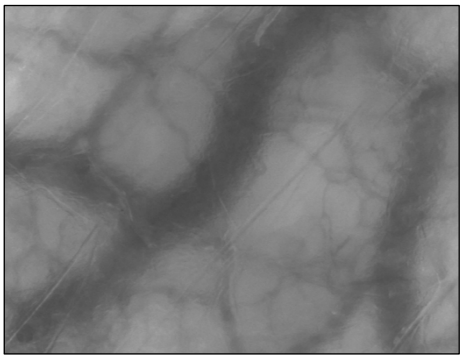

Figure 9: SDF imaging picture of a participant`s cutaneous ear vessels

The picture was converted digitally and contributed to a short video of the cutaneous microcirculation. The GlycoCheck™ Glycocalyx Measurement Software automatically evaluated quality and calculated microvascular variables including PBR [29, 95].

2.5.2 Sidestream Dark Field Imaging

Functional principle

The functional principle of SDF imaging is based on the physical phenomena that RBCs absorb light of a specific wavelength, while the surrounding tissue scatters it. This distinction of light is detected by collecting the backscattered light and is visualized in a picture of black blood vessels embedded in white tissue (Figure 9) [96].

More precisely, hemoglobin is the absorbing molecule. The maximal effective absorption due to an equal amount of light absorption in oxygen carrying and unloaded hemoglobin (“isosbestic point”) can be seen best at the wavelength of ~ 420 nm and ~ 810 nm. Using a wavelength of 420 nm would be limited to superficial vessels due to lower tissue penetration, and a wavelength of ~ 810 nm would result in a blurry picture. The wavelength of 520 nm was used for the SDF-camera (MicroScan, MicroVision Medical B.V., Amsterdam, The Netherlands) as this isosbestic point has an acceptable, effective absorption with a sufficient depth of penetration [29, 96]. Polarization is needed to reduce possible scattering of light with a different wavelength. In SDF imaging, that light is emitted by 6 LEDs that are positioned at the outer circle of the camera. After light is scattered in the tissues and absorbed in RBCs, backscattered light is magnified 5 times and detected by a central inner lying CCD (charge-

coupled device) camera. The CCD camera has a frame rate synchronic to the pulsatile light emission. A black/ grey/ white image of the vascular network is captured (Figure 9 and 10) [29, 96].

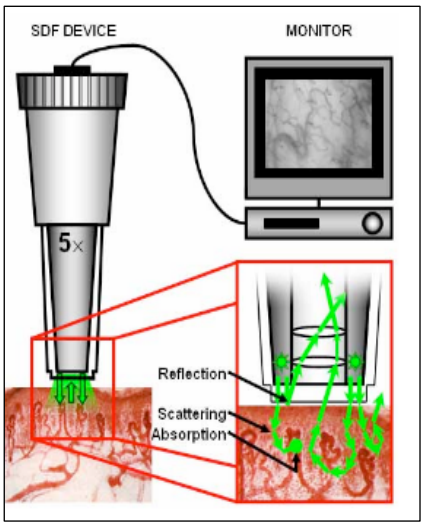

Figure 10: SDF Imaging setup. Green light is emitted from the outer ring, scattered in the tissue and absorbed of RBC (dots). Backscattered light is magnified 5x, and detected by the camera, resulting in a white/ grey picture (29)

This setup provides two improvements to OPS-Imaging, its predecessor: the straight reflections of the skin are not detected by the inner lens and synchronic light emission and CCD recording provides imaging of continuous motion of blood flow (stroboscopic effect). The stroboscopic effect reduces blurring of flowing RBC [29, 96].

The visualization technique resulted in an optical resolution of ~ 1.3 µm/pixel, so the picture frame of 720×567 pixels visualizes 0.94 x 0.75 mm [97].

Setup

The hardware required for visualization of the SDF-camera gained information, is illustrated in Figure 11 [97].

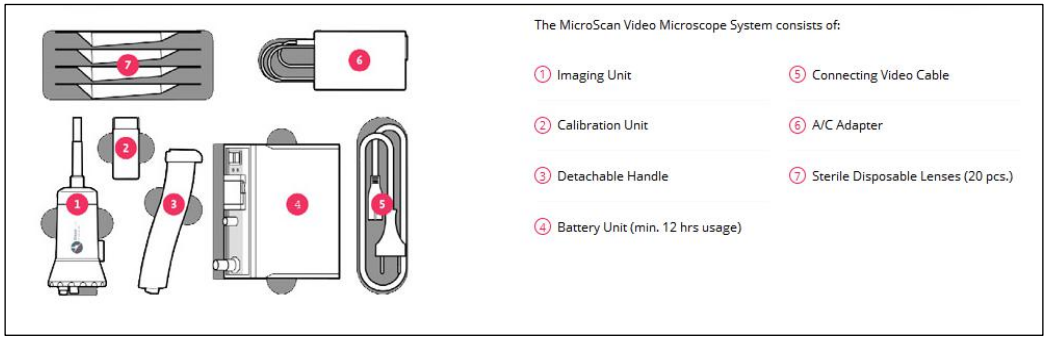

Figure 11: Former version of MicroScan (MVM B.V.) Video Microscope System set up (97). In our version the A/C adapter (symbol 6) was not needed anymore.

In the used version, the pictured A/C Adapter was not necessary anymore and videos were directly recorded into the PC (Cooler Master Technology Inc., New Taipei City, Taiwan).

2.5.3 Microvascular analysis

Measurement

Calibration of the camera was necessary before starting a new session of measurements. In order to start recording, a steady picture with sufficient light intensity and focus was required, which was set manually while holding the camera stable on the infant's ear. Two different raters conducted the microcirculatory measurements. In a parallel study, a Bland-Altman comparison test was run showing good inter-rater correlation in PBR. PBR average was compared to the PBR difference between the conductors and it was detected that there was no influence of the conductor on PBR (Bias 0.06, SD Bias 0.15, 95% limits of agreement: -0.2- 0.36). Manual adjustments and acquiring a stable picture of sufficient quality could sometimes hinder measurements. A drop of saline was put on the skin, which improved the quality of the picture due to less skin reflection. Air bubbles between camera and skin invoked an alarm that prevented recording. The recording itself only lasted a couple of seconds. The GlycoCheck™ Glycocalyx Measurement Software (version V1.2.7.7394 / Release 1.2., GlycoCheck B.V., Maastricht, Netherlands) fully mediated the recording, i.e. it started automatically as soon as the image quality was sufficient. It finished when it detected at least 3000 vascular segments of blood vessels with a diameter between 5 to 25 µm. The definition of a vascular segment is a 10 µm long segment of a vessel. The software recorded 40 frames (25 frames per second) of a single area of 300 vascular segments per average [30, 95]. To gain 3000 vascular segments, the picture frame was shifted slightly to capture in total 10 areas to complete one measurement. Each measurement session consisted of at least 3 single recordings per patient.

As preterm newborns were measured, the measurements had sometimes to be performed under difficult conditions, for example, while the preterm was under mechanical ventilation, in special positioning (prone or side positions) or lying in incubators with high humidity.

Recorded data

After recording the necessary number of vascular segments, the software performed an automated validation of these segments. For this purpose, the vessel segments in the first frame of the video clips were divided by 21 perpendicular line markers with 0.5 µm distance (Figure 12D). Each vessel segment was only valid when showing enough contrast in more than 60% out of these 21 validation points (Figure 12B). Valid vessel density can be derived as:

VVD = (number of valid vascular segments x 10 µm)/ area of tissue visualized (mm^2) [30].

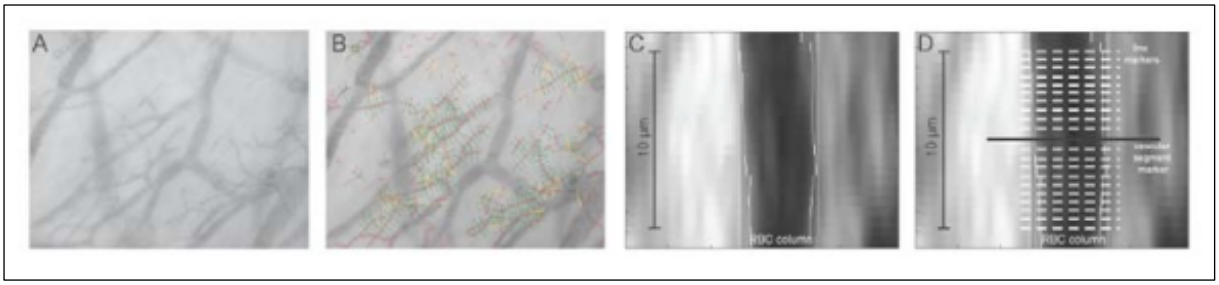

Figure 12: Validation of microvessels for evaluation. A: original frame. B: frame with validated vascular segments (green: valid, yellow: invalid). C: Single enlarged vascular segment D: Illustrated enlarged vascular segment with its 21 perpendicular line markers (98)

Further RBC filling was derived to quantify perfusion. RBC filling (%) is the proportion of perfused vascular segments with RBC present in all 40 frames compared to the total number of detected vascular vessels [30].

Calculating PBR as an inverse surrogate gauge for GCX was the next step. PBR is considered to resemble the luminal part of the GCX that is accessible to RBCs. Physiologically, only minor lateral RBC undulations occur, as in general RBC are confined in the middle of the vascular column (= median RBC column). The perfused vessel diameter (= D_{PERF}) sums up the median RBC column and the lateral RBC movements (Figure 14).

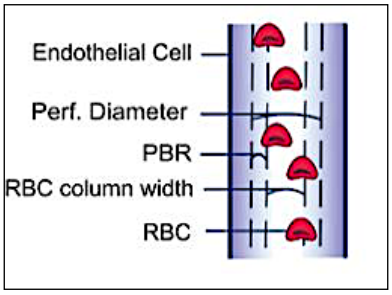

Figure 13: Visualization of microvascular RBC flow. RBC flow is mainly confined within the median RBC column. Only minor lateral undulations into the PBR (perfused boundary region of the GCX) occur. DPERF is defined as median RBC column width+ 2 PBR (30).*

Off note, it is crucial to remember that PBR represents inversely GCX size, a healthy GCX is dense with only a shallow intrudable part (so PBR is low).

Based on the considerations of Figure 12 and 13, PBR was extracted by the GlycoCheck™ Glycocalyx Measurement Software. Light intensity profiles were drawn along every vascular segment, throughout a set of 40 frames along the above-mentioned 21 line markers (840 profiles per vascular segment). The software processed the information to gain a cumulative light/ contrast distribution (=light intensity profile, Figure 14 left side). A quality check was imposed at this step, as the software screened for aberrations in the intensity profile [95]. The median RBC column width is derived from the light intensity profile as full width at half maximum (FWHM). (Figure 14, left side). Following, the slope between 25 to 75% of light intensity was extrapolated by linear regression to derive D_{PERF} (= linear

regression intercept with x-Axis. Figure 14, right side) [98]. PBR was then calculated as PBR = (D_{PERF} - RBC median column width)/ 2 (Figure 13 and 14, right side) [30, 95].

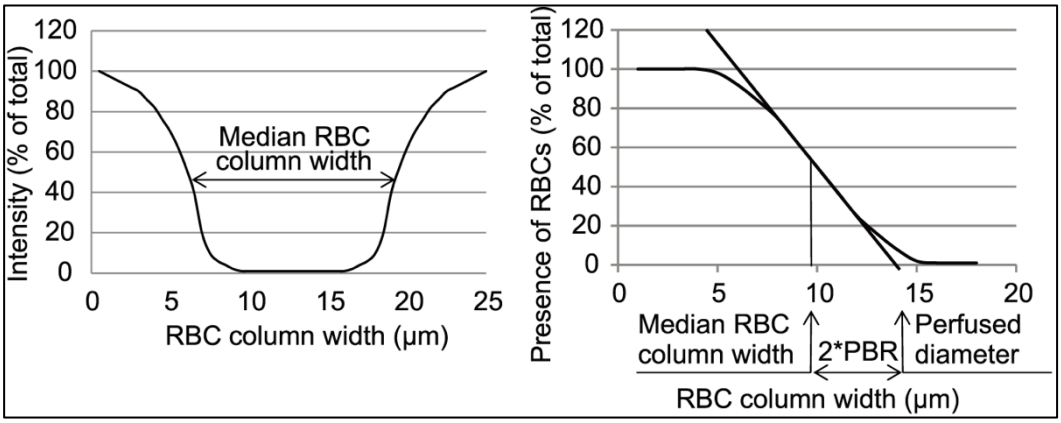

Figure 14: Calculating PBR. Left: Light intensity profile of RBC columns in vascular segments. Right: extrapolation of the vascular segment's intensity profile to calculate the perfused diameter, median RBC column and perfused boundary region (30).

2.6 Statistics

The statistical data were calculated and the graphs were drawn with either Microsoft® Excel or GraphPad© Prism v.5 (© 1995-2018 GraphPad Software, Inc.). For all calculations, the p-value of statistical significance was set at 0.05.

Before each statistical analysis, D'Agostino's test for normality was run to check for Gaussian distribution. Due to small sample sizes, Gaussian distribution could sometimes not be checked and was hence not assumed.

While focusing on the distribution of one parameter at a specific time, mean, confidence interval (CI) and standard deviation (SD) were checked. When experimental microcirculatory data were assessed, median and maximum/ minimum were used and were illustrated in Box plot as medians and whiskers. The longitudinal evaluation of clinical, laboratory and microcirculatory parameters was approached, using two-tailed paired t-test (normality was given) or Wilcoxon signed-rank test (missing Gaussian distribution) to assess changes within individuals over time (first vs. last measurement). Possible correlations between different parameters were checked with Pearson correlation or Spearman depending on D'Agostino's test for normality [99].

Furthermore, subgroups (stratified by gestational age at birth) were statistically compared. If a value in two different subgroups was compared, mostly an unpaired two-tailed t-test was run, alternatively Mann-Whitney U test was chosen. More than two subgroups were evaluated with a one-way analysis of variance (ANOVA) or a Kruskal-Wallis test in case of non-Gaussian distributed subgroups. Post hoc test for ANOVA was Bonferroni's and Dunn's for Kruskal-Wallis.

Linear regression was run to check for age dependent PBR changes by Stata 15.1. (StataCorp. 2017. Stata Statistical Software: Release 15. College Station, TX: StataCorp LLC.).

3 Results

3.1 Study population

A total of 39 preterm babies were included in the study. The mean gestational age at birth was 30w + 2d with a range of 13 weeks (min./ max.= 23w/ 36w). Figure 15 shows the distribution of gender and gestational age at birth. Male (n = 16) had a mean age of 31 ± 4 w, female of 30 ± 4 w (n = 23). There was no statistically significant gender-based gestational age difference.

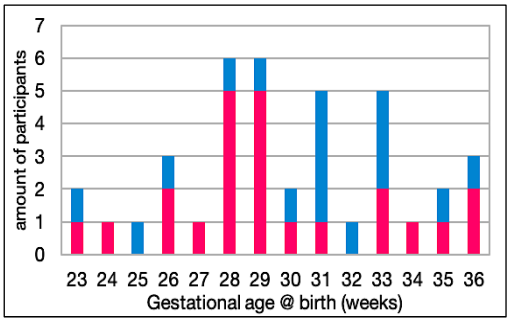

Figure 15: Participants stratified to gender (red – female, n= 23; blue – male, n= 16) and gestational age at birth

Study design stratified all 39 participants by gestational age at birth into two groups: group A, including children born with a gestational age up to 29w + 6d, and group B, including children born from 30w + 0d till 36w + 6d. Eighty-five babies born in or above the 37th completed gestational week in a parallel study, served as control group. Characteristics are presented in Chart 3.

	Group A: Gestational age at birth < 30w + 0d	**Group B: 30w + 0d ≤ gestational age at birth < 37w + 0d**	**Control group: gestational age at birth ≥ 37w + 0d**
Total amount	20	19	85
Female vs. male	15 vs. 5	8 vs. 11	43 vs. 42
Gestational age at birth (mean, SD)	27.6w (SD = 2w)	33.4w (SD = 2w)	40w (SD = 1 w)
Weight at birth; SGA* (mean, SD)	995 g; 1 (SD = 286g)	1944g; 1 (SD = 434g)	3512g; 5 (SD = 448g)
Body length (mean, SD)	36 cm (SD = 4 cm)	43 cm (SD = 3 cm)	52 cm (SD = 3 cm)
C-section	17 (85%)	11 (57%)	17 (20%)
Apgar (1st/ 5th /10th minute of life)	6.6/ 7.7/ 8.9	7.8/ 9.3/ 9.6	9.0/ 9.8/ 10

CHART 3: STUDY POPULATION AT BIRTH ACCORDING TO STRATIFIED GROUPS (A, B, CONTROL), LEGEND:* SGA= WEIGHT AT BIRTH < 10 PERCENTILE FOR GESTATIONAL AGE [100]

The most common reasons for preterm birth were premature labor (n= 23) and premature rupture of membranes (PROM, n= 21). In addition, 11 times cervical insufficiency was documented. The study included in total 6 cases of mothers suffering from HELLP- syndrome, pre-eclampsia and pregnancy related cholestasis. One set of triplets and 8 twin pairs participated.

3.2 Number of measurements and follow-up

Longitudinal study design resulted in a set of measurements. These follow up measurements were conducted to examine possible longitudinal changes. The starting point was planned to be around the time of newborn screening (NS: 36-72 hours after birth) with follow-up measurements around every completed postnatal week (i.e. NS, 1st week, 2nd week, 3rd week …).

In total, 137 measurement sessions were run while 109 were finally used for further statistical evaluation (Figure 16). The reason for not including all measurements was that some were out of schedule measurements either following blood drawings or correlated to red blood cell transfusions (obtained for another study), which could not be fitted in the set follow up scheme. In addition, one value was not used as it was an extreme outlier with more than 3x standard deviations.

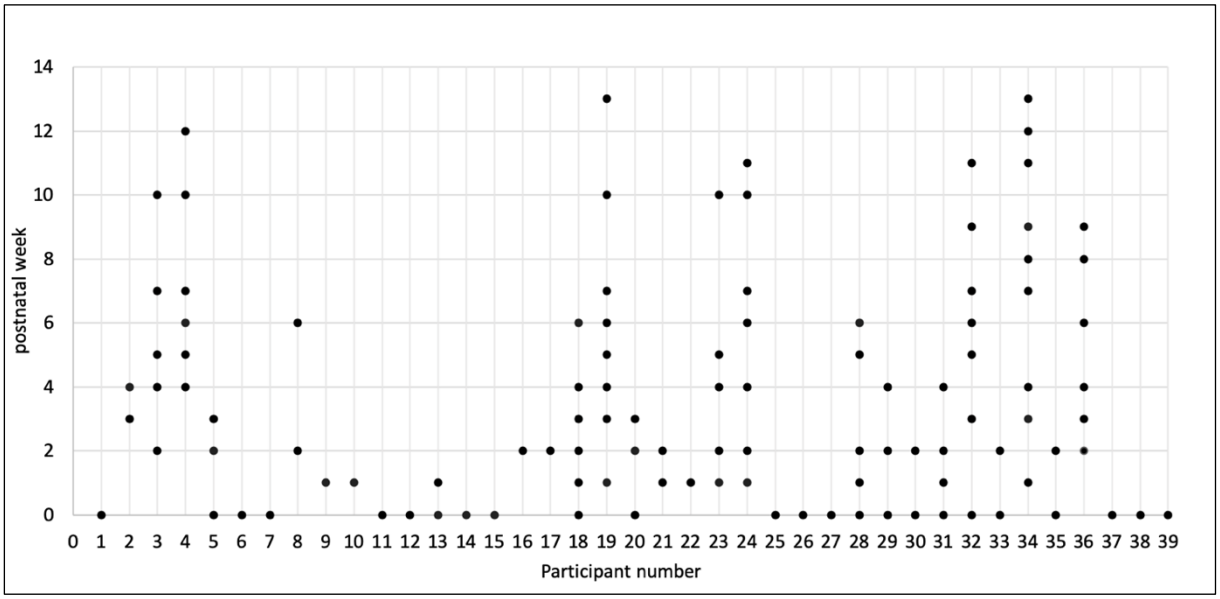

Figure 16: Overview of 109 measurements used for further calculations. Follow-up per child (x-axis: child 1-39) and postnatal time point of the measurement (y-axis: postnatal weeks, 0 is the time at the newborn screening)

Each child was measured on average three times (SD = 2), at least once, and at most 9 times (95% - CI: 2-4).

The average number of participants per measurement time point was 8 (SD = 6). Two was the minimal number of data samples (i.e. number of different participants) for a regular time point. The maximal number of participants for a regular time point was obtained at the newborn screening (NS), which was conducted in 24 out of 39 participants (95% - CI of 5 - 11).

3.3 Laboratory and clinical data

As for many of the study participants, more than one measurement session was conducted, and the sampled corresponding data (BGA, VP) was large. To asses longitudinal changes, the values obtained at the first measurement (FM) of a neonate were compared to the last measurement (LM) if at least 3 measurements per neonate were acquired. Mean age at FM was 1w (SD= 1w, min./ max.= NS/ 4w)

and 7w at LM (SD= 3, min./ max.= 3w/ 12w). Every measurement session was planned to be co-acquired with a recent blood sample, but due to organizational reasons in three cases, measurement sessions took place without complete corresponding blood samples.

Focusing on hematologic and metabolic parameters, there was a significant reduction in hematocrit, hemoglobin levels, and bilirubin between first and last measurement in 13 neonates (Chart 4). Blood glucose and blood lactate levels did not change significantly between the samples of first versus the last measurement but showed a trend for decrease.

	Newborn screening (n = 24)	**First measurement (FM, n = 13)**	**Last measurement (LM, n = 13)**	**p-value (FM vs. LM)**
Hemoglobin (g/dl)	16.7 ± 2.1	15.3 ± 2.6	10.6 ± 2.5	0.001*
Hematocrit (%)	51.0 ± 6.2	46.8 ± 7.8	32.7 ± 7.6	0.001*
Bilirubin (mg/dl)**	7.3 ± 2.0	6.6 ± 4.3	2.9 ± 1.9	0.005*
Glucose (mg/dl)**	83 ± 24	99 ± 23	83 ± 23	0.15
Lactate (mmol/l)	2.0 ± 0.6	1.8 ± 0.6	1.5 ± 0.5	0.12

CHART 4: HEMATOLOGIC AND METABOLIC PARAMETERS (MEAN ± SD), TABLE LEGEND: FM/LM= FIRST / LAST MEASUREMENT TIME POINT IN A PARTICIPANT THAT WAS MEASURED AT LEAST THREE TIMES, * $p < 0.05$ FOR SIGNIFICANCE, ** NON- GAUSSIAN DISTRIBUTION.

Postnatal changes were partially observed for acid-base homeostasis with significant increases in bicarbonate and base excess between first and last measurement ($p<0.001$). Levels of pCO_2 and pO_2 showed a non-significant tendency to increase (Chart 5).

	Newborn screening (n=24)	**First measurement (FM, n=13)**	**Last measurement (LM, n=13)**	**p-value (FM vs. LM)**
pH	7.37 ± 0.05	7.34 ± 0.05	7.37 ± 0.05	0.17
pO_2 (mmHg)	38.0 ± 10.0	32.5 ± 9 .8	36.7 ± 6.2	0.18
pCO_2 (mmHg)	40.2 ± 6.8	42.6±9.0	48.3 ± 6.9	0.09
Base excess (mmol/l)	-1.6 ± 2.2	-2.4 ± 2.5	2.3 ± 1.8	< 0.0001*
HCO_{3-} (mmol/l)	23.1 ± 2.5	21.7 ± 1.6	26.0 ± 1.7	< 0.0001*

CHART 5: ACID-BASE HOMEOSTASIS, TABLE LEGEND (MEAN ± SD): FM/LM= FIRST / LAST MEASUREMENT TIME POINT IN A PARTICIPANT THAT WAS MEASURED AT LEAST THREE TIMES POINTS, * $p < 0.05$ FOR SIGNIFICANCE. ALL PARAMETERS WERE GAUSSIAN DISTRIBUTED.

Trends for increase in hemodynamics were seen in blood oxygen saturation (SpO_2) and respiratory rate (RR). Heart rate (HR), mean arterial pressure (MAP), perfusion index (PI) and temperature did not change (Chart 6). In total, only 20 sets of vital parameters were documented at newborn screening. Stable near term infants were not monitored continuously, in four cases this led to missing values.

	Newborn screening (n=20)	First measurement (FM, n=14)	Last measurement (LM, n=14)	p-value (FM vs. LM)
HR (bpm)	155 ± 17	157 ± 15	156 ± 14	0.91
MAP (mmHg)	44 ± 7	42 ± 6	46 ± 6	0.66
RR (breaths per minute)	44 ± 12	51 ± 11	57 ± 15	0.12
SpO_2 (%)	97.1 ± 2.5	97.6 ± 1.9	98.4 ± 1.5	0.1
Temperature (°C)	36.9 ± 0.3	36.9 ± 0.2	36.8 ± 0.9	0.81

CHART 6: HEMODYNAMICS AND OXYGENATION (MEAN ± SD), TABLE LEGEND: FM/LM= = FIRST / LAST MEASUREMENT TIME POINT IN A PARTICIPANT THAT WAS MEASURED AT LEAST THREE TIMES POINTS, * $p < 0.05$ FOR SIGNIFICANCE. ** NON- GAUSSIAN DISTRIBUTION

The patients were screened for possible systemic infections by cut-off values for CRP > 0.5 mg/dl and IL-6 > 50 ng/l. From the results, significant elevation of CRP was found in 11 measurements with one-time CRP elevation found in four children and repeated elevations in two children (3, respectively 4 times). CRP > 2 mg/dl indicating neonatal sepsis in accordance to NeoKISS criteria [101] was only found in the two children with repeated CRP elevations. Interleukin-6 (IL-6) was elevated in 14 cases with three children exhibiting repeated increased IL-6 levels (2, 3 and 4 times). At birth, eight IL-6 elevations were observed, which were followed in 4 cases with an increase in CRP. Due to small sample sizes, these results were not used for further statistical correlation.

3.4 Microcirculatory data

3.4.1 Perfusion Boundary Region: Gestational and postnatal development

Data in 3.3 revealed fractional effects of postnatal development through the studying of longitudinal descriptive differences in hemodynamics, acid base, and hematological markers.

The outcome hints at how postnatal age and gestational age influenced the perfused boundary region (PBR). The influence of gestational age and postnatal age on PBR was determined in descriptive terms, later the influence of both parameters on PBR was calculated in a linear regression analysis. The assumption was that the postnatal age could hint at the extra-uterine development, whereas the gestational age could represent the intrinsic and ontogenetic development.

Before evaluating the effects of gestational age at birth, postnatal age and possible interactions between the two on PBR development, both effects are described based on the descriptive approach.

PBR changes between first and last obtained measurement

PBR: Significant FM vs. LM Change?

Since changes between first and last measurement were the main approaches to encode parameter changes as discussed in chapter 3.3, a similar approach was applied to evaluate PBR from participants with at least two measurements (n=21) or at least three measurements (n=14). In both cases, there was a significant increase from first to last measurement as determined by paired t-test, with p = 0.0006 (at least two measurements) and p= 0.0004 (at least three measurements) respectively.

LM-FM PBR difference – correlation with LM-FM clinical and laboratory parameters?

Correlations between PBR changes to changes in other parameters were further explored using the descriptive approach. The approach helped to compare the first with the last measured value. The values of 13 (BGA and metabolic samples) or 14 (VP samples) participants with more than two measurements, which changed significantly over time, were explored. The parameters evaluated were bilirubin, hemoglobin/ hematocrit, base excess and HCO_{3-}. There was no correlation between PBR and those parameters at FM and LM.

PBR at the time of the newborn screening

Newborn screening (NS) was set as the starting point of measurements indicating PBR shortly after birth. Shown in Figure 17, not all participants could be measured during the time of the newborn screening. Delayed start of measurements was mostly due to medical and technical reasons, because part of the participants were judged as clinically too unstable during the first postnatal days (most notably in the group of very premature participants).

The median PBR was 1.88 µm (min./ max.= 1.59/ 2.38 µm) and mean age was 32 gestational weeks (SD= 6w, min./ max.= 25/ 37w) in all preterm neonates. The following data were obtained at NS in stratified groups:

At NS, group A had a mean age of 29 gestational weeks (SD = 1.4w, n= 10 neonates, min./max.= 25/ 30 w), group B 34 weeks (SD = 2w, n= 14, min./max.= 32/ 37w), and the control group 40 weeks (SD = 1w, n= 85, min./max.= 37/ 42).

The set stratification showed significant PBR differences at NS between the three study groups by a one-way ANOVA (p = 0.004). Group A offered the lowest PBR values (n= 10 children; PBR= 1.8 µm / 1.6-2.2 [median/ min-max]) compared to Group B (n= 14 children; PBR= 1.9 µm / 1.6-2.4 [median/ min-max]), and the control group (n= 85 children; PBR= 2.0 µm / 1.5-2.7 [median/ min-max]) with the highest PBR values at birth (Figure 17). Dunn`s post hoc test was significant between group A and control, as well as between group B and control.

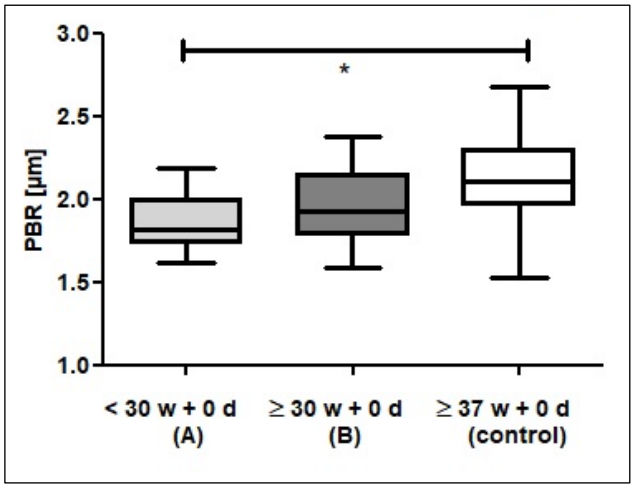

Figure 17: Box plots (median, whiskers: min-max) of PBR (µm) at NS in very premature children (group A, n= 10 participants, gestational age at birth below 30w + 0d), premature children (group B, n=14 participants, gestational age at birth between 30w + 0d and below 37w + 0d) and mature children (control group,n= 85 participants, born from 37w + 0d) with significant differences according one-way ANOVA (p= 0.004)

As the results clearly showed differences between the groups, possible confounders were checked. Vital parameters (VP), except for temperature, were not regularly obtained in our control group. Hence, in all the three groups, weight at birth, hematocrit (Hct), blood sugar, temperature and prevalence of C-sections were compared. Not surprisingly, birth weight was significantly different between group A, B, and control ($p< 0.0001$ in Kruskal-Wallis), with significant difference A and B vs control in Dunn`s post hoc test). Furthermore, birthweight and PBR at NS were significantly correlated in a Spearman correlation ($r= 0.37$, $p< 0.0001$). Hematocrit was also significantly different ($p= 0.0001$) in a one-way ANOVA with significant Bonferroni post hoc test between group B and control. Interestingly, group B had the lowest Hct values (n= 13 Hct values in total, three capillary and 10 venous samples; mean= 49%, SD= 1%), which were slightly higher in group A (n= 10 Hct values in total, only venous samples; mean= 53%, SD= 8%). The highest values were found in the control group (n= 80 Hct values in total, 35 capillary, 43 venous and 2 unclear samples; mean= 59%, SD= 8%). Pearson correlation showed a weak association between all Hct values and PBR at NS ($r= 0.2$, $p= 0.047$). When only venous samples were included, sample size shrank to 63 neonates with a similar one-way ANOVA result ($p= 0.0084$), but a Pearson correlation between PBR and venous Hct could not be detected anymore. The results obtained through one-way ANOVA were further significant for the groups in blood sugar ($p< 0.0001$) and bilirubin levels ($p= 0.0061$) showing weak correlation with PBR (Blood sugar: n= 103; $p= 0.05$; Pearson $r= 0.2$. Bilirubin: n= 96; $p=0.02$; Pearson $r= 0.2$). Temperature was also significantly different between A vs. B vs. control (Kruskal-Wallis analysis, $p= 0.0018$).

C-sections were the mode of labor with 85% in group A, 58% in group B, and only 20% in the control group. As mode of delivery did not influence PBR in the parallel study of mature neonates (n=85), it was not further evaluated as a possible confounder.

In group A and B, additional VP were documented (n (A) = 10 vs. n (B) = 9 obtained VP measurements at NS). In group B, VP in five participants could not be recorded for organizational reasons at NS. Heart rate, mean arterial pressure, and oxygen saturation were compared between A and B, and all comparisons did not show statistical relevance.

Postnatal development of PBR

First, postnatal longitudinal development was approached. Therefore, all measurements in premature participants were stratified according to their postnatal age, independent of their gestational age. To enhance statistical significance, the measurements of two adjacent time points were combined for lager sample sizes (Figure 18).

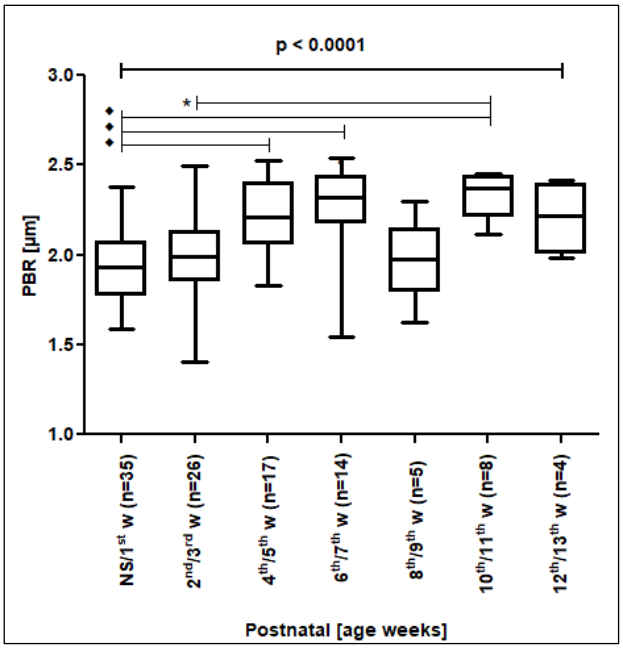

Figure 18: Box plots (median, whiskers: min-max) of PBR (µm) and its development when measurements from two adjacent postnatal weeks were combined (n= sample size of participants). LEGEND: Dunn`s post hoc test was significant against NS/1st w (◆) or/ and against 10th /11th w (*)

Figure 18 shows a general significant increase in PBR size with increasing postnatal ages (n=109, Kruskal-Wallis $p < 0.001$). PBR was significantly different in Dunn`s post hoc test between the measurements NS/1st vs. 4th/ 5th, 6th/ 7th, and 10th/ 11th completed postnatal weeks and between 2nd/ 3rd vs. 10th/11th completed postnatal weeks.

In relation to the chapter *PBR at the time of the newborn screening* (p. 29), comparison at NS showed a difference in PBR in group A vs. B vs. control group. During postnatal development PBR difference was hinted further up to the completed 3rd postnatal week between groups A versus B (Figure 19).

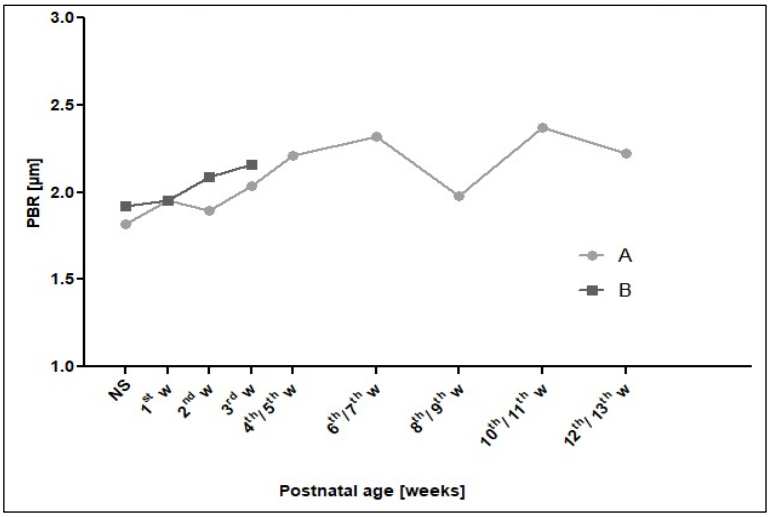

Figure 19: Median PBR (µm) and postnatal development in group A (gestational age at birth <30w+0d) vs. B (gestational age at birth ≥ 30w+0d). Only data points with two or more participants per group and time point (NS, 1st till 13th completed postnatal weeks) are shown (Chart 9)

Comparison was done only up to the completed 3rd postnatal week as in group B, only one participant was measured at the 4th postnatal week. (Chart 7).

	NS	1st w	2nd w	3rd w	4th /5th w	6th/ 7th w	8th/ 9th w	10th/ 11th w	12th/ 13th w
A	10	8	12	6	17	14	5	8	4
B	14	3	6	2	-1	-	-	-	-

CHART 7: NUMBER OF PARTICIPANTS MEASURED AT NS AND FOLLOWING COMPLETED WEEKS (W) SINCE BRITH IN GROUP A AND B

After the 4th completed postnatal week, PBR increased further in group A. Tbpdhe values converged descriptively to a steady state similar to the higher B values gained at earlier postnatal age. In group A at 8th/9th completed week, low PBR values were observed without any detectable reason. If group B showed a similar PBR increase over postnatal time or converged to a similar level, could not be tested due to the study design: participants of group B were usually not observed over the same length of time because they were discharged earlier from hospital.

Effect of gestational maturation

Measurements were afterwards grouped according to corrected gestational age at measurement, independent of postnatal age. A significant increase in PBR towards higher corrected gestational age was detected (Kruskal Wallis: p= 0.014; Dunn`s post hoc was not significant) and underlying data was stratified again according group A vs. B (Figure 20).

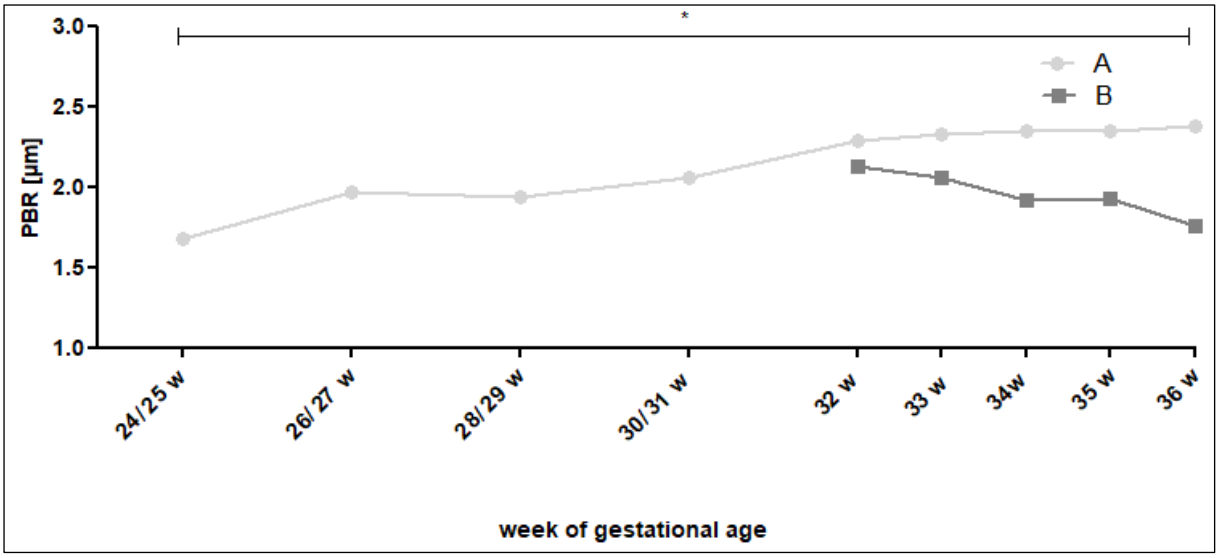

Figure 20: Median PBR (µm) according to corrected gestational age (completed weeks) in group A (gestational age at birth <30w+0d) vs. B (gestational age at birth ≥ 30w+0d). Increase in group A was significant from week 24-36 (p= 0.0004), group B was without a significant development. Only data points with two or more participants per group and gestational age were included.

In group A as shown in Figure 20, there was a significant increase in PBR size over time (n(PBR) = 78 obtained measurements; p (Kruskal- Wallis one-way ANOVA) = 0.0004). In group B, there were no significant PBR changes with increasing corrected gestational age (n(PBR) = 20 measurements). However, looking at the change of PBR in group A beyond gestational week 32 in analogy to group B, no significant increase was seen by ANOVA (n(PBR) = 27 measurements).

Interestingly, comparing PBR values between group A and B from the corrected 32nd week onwards, showed a trend for higher PBR values in group A despite lower PBR at NS. Due to the small sample sizes in each subgroup a statistical analysis was not performed (chart 8).

	24th /25th w	**26th /27th w**	**28th /29th w**	**30th/ 31st w**	**32nd w**	**33rd w**	**34th w**	**35th w**	**36th w**	**37th w**	**38th w**	**39th w**
A	3	9	21	18	8	3	7	4	2	1	4	1
B					9	6	4	5	3	1	-	-

CHART 8: NUMBER OF PARTICIPANTS ACCORDING TO GESTATIONAL AGE (WEEKS) IN GROUP A VS. B

In general, the assumption was made that increasing maturity independent of postnatal age also contributes to bigger PBR and inversely, decreased GCX size. Moreover, this increase was mainly visible in the early gestational weeks. In addition, accelerated extra-uterine PBR increase/ decrease in GCX, were considered.

Analysis of PBR Size: Mixed effects of gestational and postnatal age

A significant PBR increase was observed in postnatal longitudinal development plus the trend that early preterm participants have higher PBR values among all participants at the same corrected gestational age. From Chart 9 those findings can also be derived descriptively from all 109 measurements.

	postnatal age (completed weeks)													
gestational age (weeks)	**NS**	**1**	**2**	**3**	**4**	**5**	**6**	**7**	**8**	**9**	**10**	**11**	**12**	**13**
24			1.4											
25	1.7			1.7										
26		1.9		1.9										
27				2.0	1.8									
28	1.8	2.1	2.1	2.1			1.5							
29	1.8	1.7	1.7		2.2	2.1								
30	2.1	2.1	1.9			2.1	2.0		1.6					
31				2.1	2.4	2.4	2.4	2.2						
32	2.1	2.1	2.1		2.2	2.3	2.5	1.7		2.0				
33	1.9		2.1			2.5		2.3	2.0	2.3				
34	1.8	1.9	1.9	2.3			2.4			2.0				
35	1.8		1.9	2.0				2.4			2.2	2.4		
36	1.8										2.4			
37	2.4										2.4	2.3	2.1	
38														2.1
39													2.4	

CHART 9: PBR GROUPED BY GESTATIONAL AGE AND POSTNATAL AGE, LEGEND: PBR SIZE STRATIFIED INTO 1.4-1.5 µM (GREEN), 1.6-1.7 µM (BLUE), 1.8-1.9 µM (VIOLET), 2.0-2.1 µM (ORANGE) AND 2.2-2.4 µM (RED)

Regression analysis on PBR

The data obtained were further analyzed by linear regression to calculate the impact of gestational age and postnatal age on the PBR development. All preterm participants and mature children of the control group were included.

First, a linear regression was run to evaluate PBR at the first obtained measurement. PBR depending on gestational age at birth and corrected for postnatal age, was approximated using the following formula: $PBR = ß_0 + ß_1 * GA + ß_2 * PN$. As expected by the one-way ANOVA at NS between A, B and control, PBR values showed significant correlation with the gestational age at birth (GA) corrected for the postnatal age (PN) as seen in Figure 21 (n= 124 premature and mature neonates, $ß_1 = 0.02$, $p < 0.001$, 95%- CI: 0.013- 0.032).

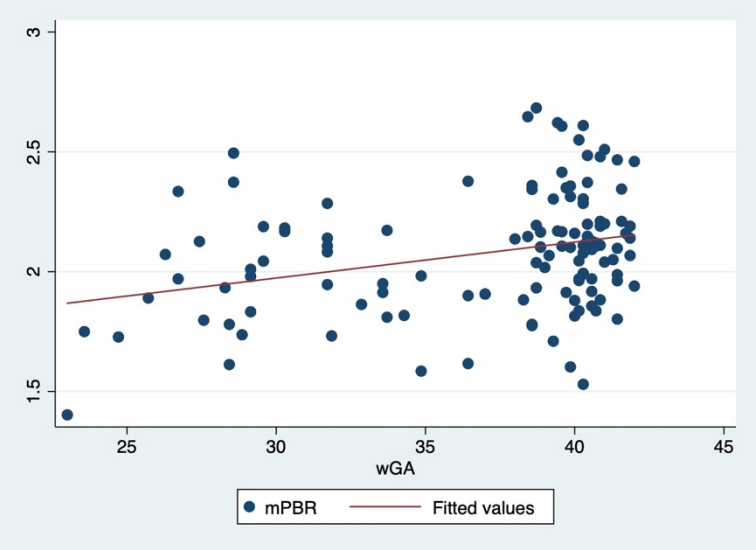

Figure 21: Two-way scatter plot of PBR at first obtained measurement (mPBR in µm) against gestational age corrected for postnatal age (wGA in weeks) with fitted regression line in red. A significant increase is shown (p p<0.001.)

Secondly, the dependence of PBR size on postnatal age was evaluated. When longitudinal development was assessed using only the first four measurements per child to provide large enough sample sizes, a significant increase in PBR size depending on postnatal age corrected for gestational age at birth was observed (n= 85 PBR values in premature neonates, ß1= 0.008, p< 0.001, 95%-CI: 0.005- 0.012 (Figure 22).

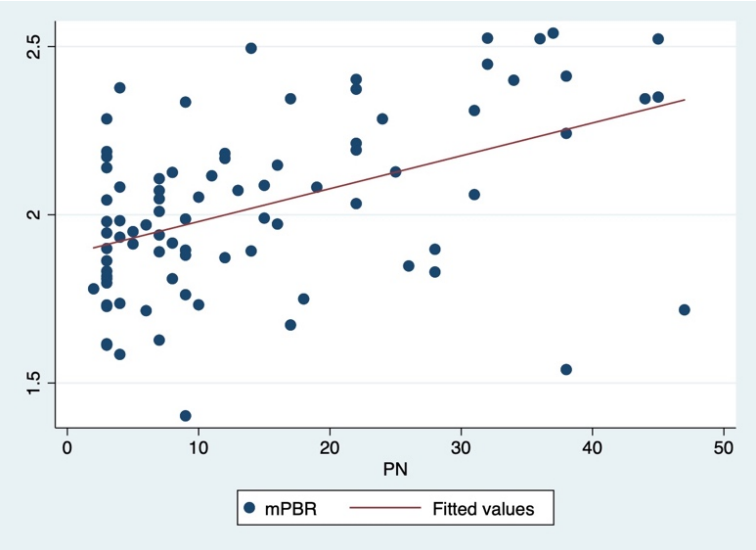

Figure 22: Two-way scatter plot of PBR at maximal first 4 obtained measurements per child (mPBR in µm) against postnatal age (PN in weeks) corrected for gestational age at birth with fitted regression line in red, which was also significantly increasing (p<0.001)

Based on both results, the descriptive results were further strengthened. How the postnatal, indicating the extra-uterine, development can be combined with the development dependent on the gestational age is focus of further evaluation.

Correlation of PBR and clinical/ laboratory parameters

As mentioned in section *PBR at the time of the newborn screening,* possible confounders were thinkable. Even though none of the parameters that significantly changed over time, correlated with PBR on FM and LM, several general correlations including all measured PBR values and corresponding clinical/laboratory parameters were detected. A general negative significant correlation was observed for all obtained hematocrit values including capillary and venous samples ($p<0.0001$, Pearson correlation coefficient r= -0.4, n= 106 measurements of PBR and Hct at the same time, Figure 23).

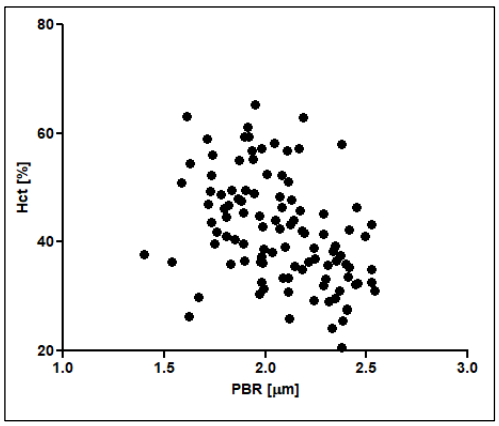

Figure 23: Hematocrit (Hct, %) vs. PBR (µm) at 106 obtained measurements with a significant Pearson correlation coefficient of R= -0.4

Interestingly, no such correlation was observed in a similar study that investigated mature newborn (personal communication). All mentioned parameters (including capillary or venous blood samples) were further checked for PBR correlation, delivering the following results:

	n-number	p- value	Correlation r
Weight at measurement	109	0.03 (S)	0.2
HR	104	0.04 (P)	0.2
RR	104	0.05 (P)	0.2
Hct	106	< 0.0001 (P)	-0.4
Bilirubin	106	0.0064 (S)	-0.3
Glucose	105	0.02 (S)	-0.2
pCO_2	107	0.0001 (S)	0.4
BE	107	< 0.0001 (P)	0.4
HCO_{3-}	107	< 0.0001 (S)	0.4

CHART 10: SIGNIFICANT PBR CORRELATION TO CLINICAL AND LABORATORY PARAMETERS, LEGEND: P FOR SIGNIFICANCE < 0.05. P: PEARSON OR S: SPEARMAN CORRELATION.

3.4.2 RBC filling

In total, 109 RBC filling measurements were used for analysis obtaining the follow results (n= 109 measurements, median= 72%, min./ max.= 52%/ 88%). Chart 11.

	Newborn screening (n=24)	First measurement (FM, n=14)	Last measurement (LM, n=14)	p-value (FM vs. LM)
RBC filling (mean, SD)	75.5 ± 7.7%	74.6 ± 7.4%	70.3 ± 9.5%	p = 0.07

CHART 11: RBC FILLING (%) AT NS, FM, LM

RBC filling showed a trend (p=0.07) but not a significant postnatal decrease when first vs. last measurement time point was compared (Chart 11). However, correlation of all 109 PBR values with the matching RBC filling values revealed a highly significant, negative relationship (Pearson correlation coefficient R= -0.88, p<0.0001) (Figure 24). RBC filling also showed a weak correlation with hematocrit (Pearson R= 0.2, p= 0.03; off note: including venous and capillary samples).

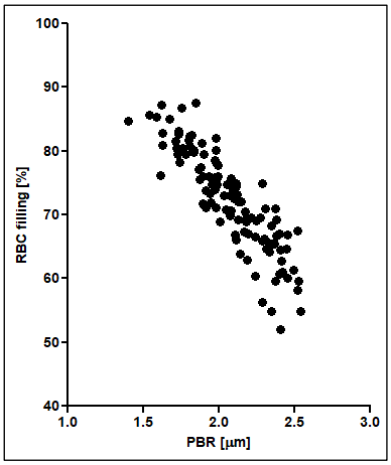

Figure 24: Correlation of PBR (µm) vs. RBC filling (%), revealing significant negative correlation (Pearson correlation coefficient R = -0.88, p < 0.0001)

4 Discussion

Previous research on microcirculation in prematurity found significant alterations compared to mature neonates [86, 102]. Secondly, increased cardiovascular risk in adolescents born premature has been described and concordant microvascular changes were found [85, 87, 103]. The increased cardiovascular risk in prematurely born adolescents might be a sequela of the observed microvascular changes in prematurity. In support of clinical findings, experimental studies with a focus on the impact of GCX have been conducted: perinatal GCX alterations impacted immediately the vascular development [77, 104]. Such aspects provided the basis to perform the study to investigate the PBR in neonates born premature and at term to assess the perinatal glycocalyx.

PBR is a well-established parameter that correlates inversely with GCX thickness [30, 105, 106]. PBR data can be calculated non-invasively in recordings from red blood cell columns undulations within cutaneous vessels with a diameter of 5 to 25 µm as discussed in sections *2.5.2. SDF Imaging* (p. 20) and *2.5.3. Microvascular analysis* (p. 22).

Multiple predetermined clinical factors were tested for possible influence over time. Since age seemed the main contributing and influencing factor, the participants were stratified by age at birth. Two groups (group A and B) based on the gestational age at birth were built. Group A consisted of very premature babies, born up to a gestational age of 29w + 6d. Group B were moderate premature infants, born beyond the 30th completed week of gestation. The influence of gestational age at birth was evaluated and further the influence of very prematurity vs. moderate prematurity in regard of the postnatal age was determined. In a parallel study, healthy term babies (control group) born with a gestational age above 37 completed weeks were measured.

At NS, the very premature group showed the lowest PBR values and the moderate premature group exhibited higher values. PBR values were the highest in the control group, which we assumed to indicate the physiological GCX size at term. In the first three postnatal weeks after the NS, group B continued to exhibit higher PBR values than group A. Interestingly, the PBR values changed when PBR development, dependent on gestational age, was compared. In group A, a significant PBR increase was observed, reaching an almost steady level from the gestational age of 32 weeks. When PBR was compared from the 32nd week till the 36th gestational week in both groups, a trend of higher PBR values in group A was described, representing a lower GCX.

The descriptive analyses led us to hypothesize that next to an intrinsically set GCX development that showed an assumed physiological decrease (PBR increase) over gestation, the extra-uterine development in very early prematurity accelerated or negatively strengthened that trend for thinner GCX more than seen physiologically in intra-uterine development (PBR increased extra- more than intra-uterine). After descriptive considerations, linear regression analysis was conducted and it

revealed similar influence of gestational age at birth and postnatal age. Including data of the control group of mature neonates, the influence of gestational age corrected for postnatal age was significant at the first obtained measurements. Also, a PBR dependence on postnatal age corrected for gestational age was shown in the first postnatal weeks.

Next to gestational and postnatal age, more parameters were analyzed. At NS, birthweight was significantly different in all three groups as expected. Temperature, bilirubin and blood sugar levels were also different between the three groups, as well as hematocrit. Further, longitudinal changes in clinical and laboratory parameters were checked for interference or confounding. The approach was to compare the first with the last gained measurement in children with a minimal number of three measurements sessions and to correlate the obtained changing parameters with PBR. Hct, bilirubin, BE and bicarbonate changed significantly over time, but none of the values was significantly correlated with PBR at FM and LM. Nevertheless, general PBR correlations, including all measurements sessions, revealed significance with those parameters and furthermore with heart rate, respiratory rate and pCO_2.

4.1 Study design

In total 109 measurements of 39 participants were included. Measurements were performed shortly after birth and with regular follow up sessions. With respect to timing, concluding on the "physiological" PBR at birth by measuring PBR values at NS is only suitable to a limited extent due to many external influences that are present in the first 36 hours of life, especially in very premature neonates. However, in order to be able to obtain a maximum of simultaneous PBR measurements and blood gas analyses also in mature neonates, the time of the NS was the best compromise.

Sample size was another constraint. Usually, prematurity is subdivided into three groups: extremely preterm (gestational age at birth below 28 completed weeks), very preterm (from 28 till completed 31 weeks) and moderate to late preterm (from 32 till completed 36 weeks) [81, 107]. Obviously, very preterm babies were less common than older ones. In addition, as mentioned, they first had to be stabilized postnatum and in order to avoid further stress by additional manipulations, the measurements were not conducted in critical situations. This contributed to missing starting or early measurements in very premature neonates. Hence, the decision was made to subdivide the samples in only two groups to obtain groups with similar sample size: neonates born below versus born from the 30^{th} completed gestational week (group A vs. B). However, sample size problems also occurred with older participants. Participants of group B were often discharged earlier from hospital when they grew up, causing an earlier study drop-out than group A.

There has been apparently no other study up to date that looked at the PBR in neonates. Even though the need for lager sample sizes is obvious, the study showed that assessment in very small neonates, even at the neonatal intensive care unit, is possible.

4.2 Methods

SDF imaging measurements and its predecessor OPS-imaging have been widely used in clinical settings to explore different aspects of microcirculation [30, 105, 106]. The neonatal intensive care unit (NICU) at the Dr. von Hauner Children's University Hospital in Munich, Germany, has investigated transcutaneous microcirculatory perfusion for variable clinical questions for more than fifteen years, highlighting the interaction between peripheral blood vessel characteristics and (patho)-physiological conditions [88, 108, 109]. There are many advantages of those methods: they are non-invasive measurements and have no radiation exposure. Measurements can be performed at bedside and have been validated at our institution and around the globe [106, 110].

Studies still explore if and to what extent cutaneous results can be conveyed to other organs, especially as the used transcutaneous SDF Imaging measurements were restricted to the skin vessels with a diameter of 5 to 25 µm [95]. So far it is known that skin microcirculation contributes strongly with its huge vascular bed to the vascular system as it is the biggest human organ [111, 112]. In neonates, the relation of surface to total body volume is higher than in older children and adults making the cutaneous circulation even more relevant [113]. Early cutaneous microcirculatory changes are seen in systemic reactions like sepsis in preterm infants [89]. Also, cutaneous microcirculatory reactions to blood transfusion in anemic premature neonates were observed even if systemic macro-circulatory parameters remained unchanged [88].

Recently, GCX gained focus by using SDF imaging technique [98, 114]. PBR measured by SDF- imaging is an indirect marker of the GCX, which visualizes the RBC accessible part of the GCX. Even though PBR and vascular assessments were correlated [30], the true nature of the GCX is only hinted by this method. Hence, interpretation of PBR values with respect to GCX function has to be handled with caution, because PBR illustrates the luminal, intrudable part of the GCX and does not allow to conclude on the full size or the composition of the GCX.

4.2.1 Measurements

Backer et al. stated the "key points for optimal image acquisition" (mostly used for the above mentioned similar studies), were closely watched and in use [115]. The key points are:

- 5 sites per organ
- avoidance of pressure artifacts
- adequate focus and contrast adjustment

- recording quality
- removal of secretions

In previous studies that were conducted at the NICU, Dr. von Hauner Kinderspital München, Germany, SDF-imaging in mature and premature babies was proved to fulfill the above-mentioned key points when assessing vessel characteristics such as functional vessel density, vessel surface and blood flow quality [86, 116]. The number of 5, (minimum 3) measurements per assessment were aimed for, depending on the participants' condition. Other aspects about the very preterm neonates were special circumstances. The partly hindering circumstances, such as uncontrolled movement of the newborns or movements due to ventilation, the limited space laying in incubators, and more, were the challenges to obtain high quality video recordings. Sleeping resulted in best quality. Long measurements sessions that would decrease incubator temperature and body temperature [110] were other reasons that resulted in time limitations.

Key points, such as avoidance of pressure artifacts, manual adequate focus and contrast adjustment, and recording quality underwent quality checks run by the software itself and recording only started when intensity and focus were of acceptable quality. Insufficient contact between camera and skin was detected when light could not overcome the camera- skin transition zone. Saline solution was used to reduce light reflection at the camera/ skin transition zone. Air bubble alarm hindered further recording and continued only when the setting was adjusted. Pressure artifacts were detected by a visible decrease of blood flow. To reduce pressure artifacts, the arms of the conductors rested on a hard foundation during video acquisition.

In adults, sublingual measurements have been conducted [28], but in neonates, this approach is difficult, as they would suckle. Commonly, the skin of the ear helix or the axilla has been used, and it has been reported that transcutaneous measurements deliver similar sufficient results. This is because the skin of newborns is still thin and the stratum corneum is not fully developed [110, 117-119]. The ear helix used for measurement in previous studies proved to be a clean and clear site in premature and mature neonates [110, 116, 120]. As both premature and mature infants were included, the ear helix was set as common measurement sites. The ear helix was also chosen because it was easily accessible in mature neonates wearing clothes compared to the inner arm or compared to sublingual acquisition due to reflective sucking.

A sterile slipcover for the camera was used, which could theoretically lead to inaccurate analysis through possible interference with the emitted light. A "slipcover effect" was recently demonstrated, where due to slip cover induced light fraction, the focus detecting small vessels was diminished [121].

Measurements were conducted by two medical students. Therefore, to check for interrater variability, nine mature infants were measured by both conductors shortly one after another, without any significant differences (*2.5.3 Microvascular analysis,* p. 22).

4.2.2 Software

The used GlycoCheck software V1.2.7.7394 / Release 1.2 required manual calibration before each measurement session and manual setting of focus and light intensity. Adjusting focus and intensity sometimes was a time-consuming necessity, which interfered with the restricted time frames scheduled for the measurements. After quality demands were fulfilled, recording started and measurements and PBR calculations ran completely automatically. The automated calculations could explain the good inter-rater reliability.

4.3 Results

Prematurely born adolescents and adults are known to have an increased cardiovascular risk [84, 85, 87]. However, the factors contributing to this increased risk profile are still under investigation, e.g. the Belgian prospective study PREMATCH (PREMATurity as predictor of Cardiovascular–renal Health) compared former premature to mature newborns in their early adolescent years for cardiovascular micro- and macrocirculatory differences [122]. Similar to Barker's fetal origin hypothesis, which postulated in the 90s that low birth weight play a crucial role in the development of cardiovascular diseases [103, 123], the PEMATCH study aims for equivalent results due to prematurity [122].

Over the last decade, studies concentrating on the microcirculatory aspect have revealed significant differences in microcirculation dependent on gestational age of birth in prematurity and compared to mature birth [86, 109, 118]. Kroth et al. found a postnatal decrease in functional small vessel density (FSVD = length of small vessels per observed skin area) in premature neonates without a change in vessel diameter within their first month of life [109]. Puchwein-Schwepcke et al. observed significantly higher functional vessel density (FVD = length of vessels per observed skin area) in preterm neonates compared to term newborns that also dropped during postnatal time. Despite higher FVD, premature infants had a lower vessel surface (= percentage of vessels to observed skin area), due to a higher percentage of small vessels (<10 µm) with a lower percentage of medium (10 to 20 µm) and big vessels (>20 to 100 µm). In neonates at near term age FVD remained higher than in mature neonates [86]. Higher FVD persisted in adolescents and adults born prematurely compared to former maturely born grown-ups [85].

The role of the GCX as an essential regulator of vascular health and integrity is increasingly recognized [13, 18, 65] and disturbances of the GCX are thus thought to contribute to micro- and macroangiopathy [69-71]. Nevertheless, the perinatal role of GCX in the field of prematurity related angiopathy has not been approached in detail.

4.3.1 PBR at birth and postnatal changes

The present study investigated whether prematurity induces measurable effects on PBR to enlighten the perinatal vascular role of GCX. As PBR is a new method to investigate GCX in neonates,

conventional, comparable values have not been established. So far, no in vivo GCX reference values could be found. In total 109 PBR measurements were gained, ranging from the 24th week of gestation up to mature gestational weeks. As PBR measurements depend on the lateral movements of erythrocytes in the vessel lumen that are restricted by an intact GCX, it decreases with increasing GCX size and vice versa.

First, PBR values at NS as the earliest set measurement point were obtained including 24 measurements with a median PBR of 1.88 µm (min./max.: 1.59/ 2.38 µm). Further comparison of three groups stratified on gestational age at birth (24-29w + 6d, 30-36w + 6d, mature babies) showed significant differences of PBR at the time of newborn screening with lowest PBR values in the most immature neonates. Based on these results, conclusion was made that very premature neonates have the biggest GCX. This result might seem surprising at the first glance, because the GCX is known to be a very delicate structure that can be damaged easily by various factors such as oxidative stress, hyperglycemia, inflammation and many more [18], all factors that are often encountered in extreme premature neonates. However, a possible explanation for the higher GCX in early gestational age could be its role in angiogenesis during early gestational ages where it is involved in anchoring of pro-angiogenetic growth factors (VEGF-R2, And2, vWF and Tie-2) through highly sulfonated GAG chains [104].

An experimental study by Henderson-Toth et al. demonstrated that the vascular GCX can be detected in quails as soon as blood flow is present. Induced shedding by HA degradation led to increased vascular leakage, “prevented vascular remodeling and resulted in a hyperperfused vascular plexus” [77], indicating that the GCX plays an important role in intact vascular development. Harfouche et al. studied the selective shedding of GCX by de-sulfonating HA, which led to micro-and macrovascular perinatal impaired development stressing further the impact of GCX shedding in vasculogenesis. They proved on stem cells and zebrafishes that by de-sulfonating GCX, even direct morphological malformation (such as shortened tails in zebra fishes) followed impaired vasculogenesis. Such changes were due to genetic modulations on (Wnt-/ Shh-) pathways that suggested a glycocalyx - gene transcription axis. The changed morphological findings were correlated to a decrease in vessel lumen with increase of small vessels and accompanied stagnant blood flow [104].

Interestingly, van Elteren et al. postulated the importance of the intra-uterine hypoxic conditions for physiological angiogenesis [118]. Antenatal intra-uterine hypoxia (pO_2 = 2.5 to 3.5 kPa) compared to higher oxygen levels in the postnatal extra-uterine environment (pO_2 = 4.0 to 9.0 kPa) could be the physiological frame for normal development of the microcirculation [118, 124, 125]. This physiological frame has very limited borders because a more pronounced hypoxia induces pathologies as observed in IUGR [118, 126]. Physiological shedding of GCX due to intra-uterine hypoxia [127] could be an

explanation of lower GCX in mature neonates compared to premature neonates and describe a maturations process.

The following questions were drawn from the results: if very premature neonates show the largest GCX/ smallest PBR and mature babies show the smallest GCX/ biggest PBR, how does the GCX/ PBR of those very premature babies develop over postnatal age? Is the extrauterine GCX/ PBR development of those very premature babies comparable to the intrauterine one?

For this purpose, we obtained weekly follow up PBR measurement of premature neonates. For further analyses, the PBR values were grouped, according to corrected gestational age and postnatal weeks of life, respectively. We detected a significant increase of PBR values with advancing gestational age, but also a significant dependence on the postnatal age. To gain information about extrauterine vs. intrauterine development, group A and B were regarded separately. Here, PBR increased significantly over time in the very premature neonates (group A) when it seemed to reach a steady state from the age of 32 gestational weeks. By contrast, in group B, starting at a corrected gestational age of 32 weeks, no significant PBR changes over postnatal time were observed. This might suggest that the 32 weeks of gestation could be the cutoff point up to which an intrinsic determination and ontogenetic program runs the GCX development.

The cut-off at 32 weeks of gestation is remarkable, because the time of 32nd/33rd weeks of gestation is known to be an important milestone in neonatal development. This is because mortality and morbidity is much higher in children born before this time [128]. Accordingly, WHO's stratification classifies preterm neonates as extremely preterm (less than 28w), very preterm (28w to 31w + 6d), and moderate to late preterm (32w to 36w + 6d) [81]. The set stratification fitted further, as even though the participants were stratified according to gestational age at birth born earlier vs. at/ later than 30th week of gestation, group B at NS only contained participants with a gestational age of at least 32 weeks.

4.3.2 Accelerated extra-uterine GCX dynamics

Both gestational age and postnatal age are determinants of the PBR as seen in this study by descriptive analyses and logistic regression. The direct comparison of PBR values between the corrected 32nd to 36th gestational week between groups A and B revealed a general trend towards higher levels in group A. Thus, the following hypothesis was extracted: the very premature babies are born with a very small PBR which increases (analogue: a large GCX that decreases) significantly, from 32 weeks of gestation their PBR appears to be bigger (GCX is smaller) than that of preterm neonates with a comparable gestational age at birth. Simplified, one could assume an extra-uterine accelerated change in PBR (GCX) in early prematurity.

Up to now, only hypotheses can be made how/ if a possible intrinsic, ontogenetic program is susceptible to the extra-uterine environment. In this context, it was recently demonstrated by plasma proteome profiling that extreme premature neonates postnatally exhibit a different kinetic in protein

level changes over time than more mature preterm neonates [129]. This might hint at an alteration of intrinsically determined functional domains by external factors in dependency of the degree of maturity at birth.

That postnatal PBR dynamics observed in group A might be cautiously interpreted as a possible extrauterine “catch up” i.e. acceleration of the physiological increase in PBR observed with advancing fetal development, but could also be expression of an increased pathological shedding of the GCX.

The phenomenon of accelerated extra-uterine growth is well known in extreme premature neonates. Extra-uterine accelerated development of growth, also called catch-up growth, has been described in premature newborns [130-137]. This term is used to describe an above average increase of body size, length, weight gain, or even head circumference in preterm newborns or newborns born small for gestational age [136]. Catch-up growth in preterm newborns is of interest as these children are more prone to adolescent overweight and metabolic diseases [135]. This acceleration in growth leads to a significantly shortened life [134]. Contrary to the metabolic aspects, catch-up growth in premature neonates, born small for gestational age and in general, led to an improved neurodevelopmental outcome [132, 133]. Catch-up growth has been proven widely to be a positive influencer of neurodevelopment [131], as higher glucose serum levels lead to a better myelination and differentiation of brain glial cells [130]. Alexeev et al. addressed this challenge in catch-up growth in premature newborns through modified rat models, which showed that catch-up growth leads to an improved neurodevelopment, but decreased insulin sensitivity [137].

The extent to which physiological “catch-up” of PBR overlaps with pathological GCX shedding in preterm babies that may contribute to vascular impairments, can only be hypothesized based on the current scientific knowledge. It needs to be discussed if extra-uterine acceleration of PBR increase, respectively GCX shedding may be the crucial step in the altered vascular development, as experimental findings implicate the importance of GCX [77, 104]. As discussed before, vascular changes were visible after induced shedding of the GCX in quail and zebrafish [77, 104].

Clinically, shedding of GCX has been described in various pathologies such as diabetes mellitus, sepsis, and more as discussed in section 1.2.5, and an increased destruction of its components was visible [66, 105, 138]. The knowledge about the GCX shedding in juvenile diabetes mellitus patients plus the known insulin intolerance in preterm newborns strengthens a possible GCX shedding due to metabolic reasons [139, 140]. Similar links of decreased GCX to sepsis are also possible as preterm neonates are more susceptible to sepsis [141]. One point to consider is lower albumin levels in premature babies that correlates with gestational age [142], a protein that has been described to stabilize GCX in septic patients [13, 75]. Another point to consider is oxidative stress, which has been discussed as the contributor to later-onset diseases in premature babies. Since oxidative stress is another GCX shedding factor, the reduced GCX maybe the link in between [13, 143].

The finding of an accelerated and disproportionately high decreases of GCX postnatally in extreme premature neonates might play a pivotal role in the vascular physio- and pathophysiology of prematurity. This is especially interesting in view of the known alterations in the microcirculatory network of preterm neonates and the increased cardiovascular risk profile of these infants in later life. However, the causal relation and the exact mechanisms contributing to vascular pathology in preterm infants deserve further investigation. Further assessments on this subject must also include other aspects of vascular development, not only the interaction of blood and GCX, but also the interactions between GCX/ endothelial cells and surrounding pericytes and other tissue components, that may possibly have an impact [144].

4.3.3 Further clinical factors on premature neonates' GCX extrauterine development

The question if or to what extent microcirculatory findings as the PBR correlate with clinical and laboratory parameters, is still not fully answered [88, 118]. Clinical parameters were highlighted in several studies, and correlation between GCX shedding and pathological clinical parameters such as high blood sugar was proven [66, 68, 139]. Van Elteren et al. demonstrated in their linear mixed model for FVD in prematurity relevant differences in vital parameters besides postnatal age that need to be included in microcirculatory assessment [118]. We could not verify differences in vital parameters, when we compared first and last measurement, but detected differences in bilirubin, Hct, BE and HCO_3. In our study, PBR overall showed a weak correlation with the four parameters that significantly changed over time, but no correlation with PBR at those single time points was found. This might be due to small sample sizes for single time points.

Likewise, increased sample size might be the explanation, why general correlations between all PBR values obtained and several parameters were indeed significant (weight, HR, RR, glucose, bilirubin, as well as base excess, pCO_2 HCO_{3-} and Hct with mixed venous and capillary samples). Plus at NS, temperature, bilirubin and blood sugar levels were also significantly different between the study groups as expected and those parameters showed a weak correlation with simultaneous PBR. An upcoming multiple linear regression analysis is going to evaluate in detail those possible effects of clinical and laboratory parameters on perinatal GCX assessment to include possible confounders besides age.

Evaluation of hematocrit raised further interest in possible methodical confounding: calculating PBR in capillaries with a decreased hematocrit may induce bigger undulations of RBC columns mimicking a higher PBR, as RBC filling is known to correlate inversely with PBR [30] (Figure 25).

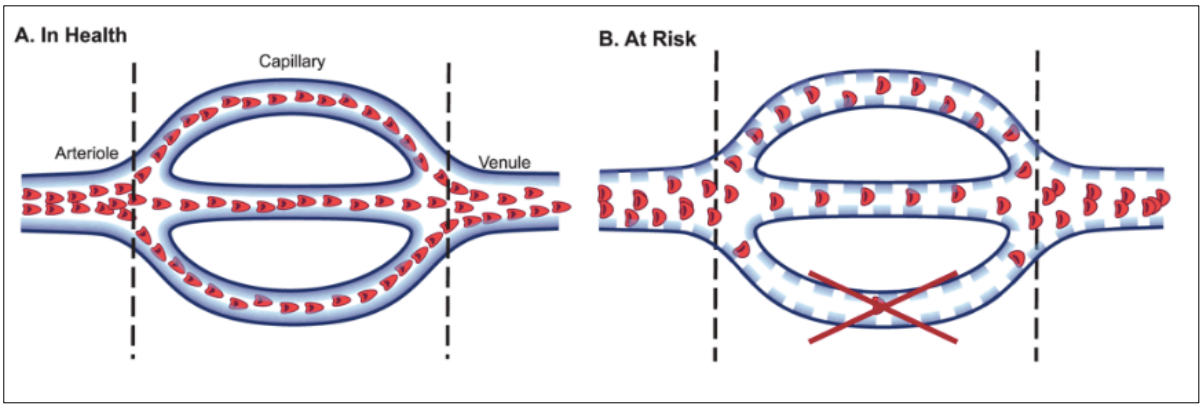

Figure 25: "Schematic illustration of the relation between glycocalyx accessibility and microvascular perfusion regulation. A) Healthy state: Intact glycocalyx prevents red blood cells (RBC, red dots) from penetrating into its domain, reflected by a low perfused bound. B) Risk State: Altered composition of glycocalyx (lined dots) allows RBCs to penetrate deeper into the glycocalyx, closer to the anatomical border of the lumen (endothelium), reflected by the high PBR. Due to the widening of RBC distribution width and volume, there is more space in between each RBC, as shown by decreased RBC filling percentage (less positive contrast per vascular segment per time point). Also, prolonged state of glycocalyx degradation leads to edematous and non-functioning vessels, leading to shorter vessel density per area of tissue (reduced valid microvascular density in risk PBR), depicted by the loss of bottom vessel." (30)

The existing literature demonstrates negative correlation of Hct with PBR in pathologies, such as systemic sclerosis [145]. Gu et al. described ethnical PBR differences corrected for hematocrit as the explored populations showed correlations of Hct with PBR [106]. In our study evaluation of PBR/ hematocrit correlation was especially challenged by the perinatal Hct dependence on gestational age [146, 147]: correlating hematocrit and PBR delivered inconsistent results depending on the evaluated time interval and/ or group sampling. In the premature group, at NS hematocrit correlated marginally positive with PBR, whereas a strong negative significant correlation of PBR and Hct could be found including all obtained values. In the mature group no significant correlation was detected at all. The reservation is backed with significant inverse correlation of PBR and RBC filling, which was strongly negative in our study. Contrarily, van Haeren et al. stated that by including automatically only valid vascular segments with a RBC filling of at least 50% (for example 11/21 line markers of a vascular segment are perfused, chapter *Recorded data, p. 22*), a possible Hct interference is eliminated [121]. In our study valid vessel segments were defined as segments with a RBC filling of at least 60%, thus a Hct interference would even be more unlikely.

Discussing methodical interference, in prematurity one could argue that a high percentage of small vessels in prematurity [86] could be a methodical errand resulting in smaller PBR values as smaller vessels might restrict RBC column undulations. The software used did not give any insight into the percentage of small, medium or large vessel diameters to rule out this methodical question. But as

Puchwein-Schwepcke et al. proved, higher percentage of small vessel in prematurity persists with higher postnatal ages even close to term age (~ corrected 34 gestational week) and it is still higher than in mature neonates [86]. However, in the present study, the postnatal PBR increased in the very premature group A up to the 32nd gestational week.

In general, the finding of significant longitudinal changes of clinical parameters is supported by other studies. Especially non-conjugated bilirubin is known to be higher in the first couple of days, hence endangering the newborns to kernicterus. This is attributed to the fact that the postnatal non-conjugated bilirubin increases, and the liver enzymes responsible for the conjugation process need time to mature [148]. The maturation progress is especially negatively affected by prematurity [149, 150]. It is also necessary to mention the increase of base excess and bicarbonate. The low starting points of bicarbonate and base excess are possible indicators of the known gestational age dependent maturation of kidney secretion of cations and re-absorption of bicarbonates. Postnatally acidosis occurs mostly in a mixed respiratory- metabolic mixture due to the decreased kidney function plus a decreased CO_2 exhalation [151].

As changes in parameters can also be just another sign of general maturation in neonates, those parameters need to be included in further evaluations for possible confounding of PBR results.

4.4 Future prospects

This study aimed to highlight the vascular role of GCX in prematurity to further examine GCX as a possible crucial factor in the perinatal determination of vascular pathophysiology. So far, experimental studies showed the importance of GCX in angiogenesis by selectively shedding the GCX and observing altered microcirculation [77, 104]. Alterations included a decreased blood flow and other microvascular patterns with smaller vessel lumen [104]. Clinically, a recent study by Puchwein-Schwepcke et al. described that premature neonates exhibited a distinct premature cutaneous vascular phenotype with a significant higher percentage of small vessels and an increased FVD compared to mature neonates [86]. A distinct microcirculatory phenotype in the born premature can be detected even during adolescence [85] and this is accompanied by an increased cardiovascular risk [85, 103].

Microcirculatory alterations are not only seen in prematurity, but also in critically ill children. An increase in buccal functional capillary density in intubated children in sepsis was associated with a higher survival rate [152]. In critically ill adults, decreased functional vessel density was also associated with higher mortality [153]. Recently, microcirculatory studies in these patients concentrated on the GCX [13]. In general, current studies that investigated the microcirculation in prematurity, or vascular assessment of former premature neonates have focused on the FVD [85, 86, 88, 89, 109, 154].

Therefore, it was the aim of the present study to enlighten perinatal GCX in premature and mature neonates.

The approach to the GCX through the indirect marker of PBR, showed significant differences at birth between very premature, moderate premature, and mature neonates. Postnatal growth had an impact of PBR increase and GCX decrease (indicating shedding) with a relevant influence of gestational age at birth. The interest was to show clinically the perinatal GCX development in premature and term neonates to improve our understanding of factors possibly underlying altered vascular development in premature neonates.

Results collected in the study give an insight, but the main question on how the endothelial GCX develops perinatally and to which extent it is involved in the development of a distinct premature vascular phenotype that marks the juncture of pathological vascular development, needs further investigation. Also, the functional consequences of altered GCX dimensions in extreme preterm neonates and a possible association with the development of pathologies such as hypertension in early adolescence need to be elucidated. A bigger sample size can strengthen the hypothesis that extra-uterine growth makes the intrinsic GCX mediated angiogenesis in prematurity more vulnerable. Furthermore, similar studies must be conducted with more participants to evaluate not only the development, but also to screen for further contributing factors.

5 Summary

The endothelial glycocalyx (GCX) is acknowledged as a pivotal juncture in the development of vascular pathologies in sepsis [73], diabetes [53, 66-68, 155], cardiovascular [65, 69-72] and other diseases. Moreover, impaired microcirculation leading to perivascular edema [27] and altered rheological behavior [15, 20-22] is likely due to reduced endothelial GCX. Perinatal alterations in GCX have been investigated in vivo and in vitro [77, 104] and functional and structural alterations of the microcirculation in premature neonates have been described in previous studies [86, 89, 109, 118]. However, now the endothelial GCX, as a possible mediator, is increasingly highlighted in understanding perinatal pathologies in microcirculatory vessel development [77, 104]. Further studies on the perinatal glycocalyx and the corresponding microcirculation were the primary aim of this study.

A prospective study was conducted including 39 premature infants born at the Perinatalzentrum Frauenklinik Maistrasse of the Ludwig-Maximilian- University, Munich, Germany. Data on the GCX in 85 mature babies obtained in a parallel study, served as control. The ethical committee of the Ludwig-Maximilian-University approved the study. The GCX was assessed indirectly by the capillary endothelial GCX perfused boundary region (PBR), an internationally validated, inverse gauge for microcirculation [30, 105, 106, 138, 145]. PBR was obtained transcutaneously using non-invasive SDF-imaging of blood flow in the microcirculation of the participants' ear helix [30]. The basic requirements for a valid image quality were guaranteed [115] and the GlycoCheck™- software automatically calculated the PBR of video segments.

Longitudinal measurements were planned at the newborn screening (NS) and run around every full postnatal week ± one day; vital und laboratory parameters were also obtained. Within a 12 hours frame before or after measurement, a blood sample was drawn and recorded. PBR measurements of premature neonates were documented in 109 cases and blood samples at the same time were obtained in 106 cases. The measurements were stratified between very premature (group A [gestational age at birth < 30w + 0d]), moderate premature (group B [30w + 0d ≤ gestational age at birth < 37w + 0d]), and mature neonates (control group [gestational age at birth ≥ 37w + 0d]). For further evaluation, the starting point at NS was approached to visualize the PBR at birth.

A significant increase between PBR (decrease in GXC size) and gestational age at birth was observed across the three groups. PBR at the first measurement after birth further significantly depended on gestational age at birth corrected for the postnatal age. This was found in all measured premature and mature neonates in a linear regression analysis. Furthermore, the longitudinal development in premature newborns showed an increase in PBR size, which we interpreted as gestational age dependent PBR changes. These changes were significant in group A, than reaching a steady plateau from 32 weeks of gestation and continued with higher PBR values compared to group B between 32nd

and 36th gestational week. Also, linear regression analysis showed a significant dependence of PBR on postnatal age in the first four follow-up measurements.

From these data a hypothesis was drawn, that the smaller GCX (bigger PBR) indicate a higher susceptibility with increased shedding of the fragile perinatal GCX in the extra-uterine environment compared to intra-uterine physiological maturation. Except for age, further possible influencing factors were tested, but none of the parameters showing a significant change over time as seen by comparing first measurement (FM) vs. last measurement (LM) correlated to PBR size at FM and LM. This could be due to small sample sizes, as general correlations could be detected when all measurements were included. The main limitations of the study were small sample size due to limited availability of stable very preterm babies, and related restrictions in follow-up measurements. Furthermore, PBR measurements only allow concluding on the size of the GXC without giving any information about its functionality.

To affirm and strengthen the findings of the present study, further investigations are needed to improve our understanding of the pathophysiology of premature newborns.

6 Zusammenfassung

Die endotheliale Glyocalyx (GCX) ist als ein Drehpunkt in der Entstehung von vaskulären Pathologien bei Sepsis [73], Diabetes mellitus [53, 66-68, 155], kardiovaskulären [65, 69-72] und weiteren Erkrankungen anerkannt. Genauer gesagt ist eine verringerte GCX wahrscheinlich der Grund für eine beeinträchtigte Mikrozirkulation, die zu perivaskulären Ödemen [27] und zu einem verändertem rheologisches Verhalten führt [15, 20-22]. Perinatale GCX Veränderungen wurden bis dato in vivo und in vitro untersucht [77, 104]. Funktionelle und strukturelle Veränderungen der Mikrozirkulation bei Frühgeborenen wurden schon vormals in verschiedenen Studien beleuchtet [86, 89, 109, 118]. Nun, gewinnt aber die GCX zunehmend als möglicher Mediator in der Entstehung der frühgeburtlich bedingten perinatalen mikrozirkulatorischen Pathologien an Bedeutung [77, 104]. Eine tiefere Betrachtung der perinatalen GCX und der dazugehörende Mikrozirkulation war das Ziel dieser Studie.

Eine prospektive Studie mit 39 frühgeborenen Neonaten wurde am Perinatalzentrum Frauenklinik Maistrasse der Ludwig-Maximilian- Universität, München, Deutschland, durchgeführt. Parallel dazu wurde eine Gruppe von 85 reifgeborenen Neonaten untersucht, die als Kontrollgruppe diente. Die Ethikkommission der Ludwig-Maximilians- Universität genehmigte die Studie.

Die Bestimmung der GCX erfolgte indirekt durch die kapilläre „perfused boundary region (PBR)“, ein international anerkannter, inverser Parameter in der Mikrozirkulation [30, 105, 106, 138, 145]. Die PBR wurde durch die Messung des mikrozirkulären Blutflusses am Ohr der Studienteilnehmer mittels einer transkutanen, nicht invasiven SDF Bildgebung ermittelt [30]. Die Grundvoraussetzungen für eine

ausreichende Bildqualität wurden beachtet [115]. Die GlycoCheck™- Software berechnete automatisch die PBR der gewonnen Videosequenzen. Für den longitudinalen Verlauf wurden die ersten Messungen zum Zeitpunkt des Neugeborenenscreenings angesetzt, mit weiteren Messungen nach je einer weiteren Lebenswoche ± einen Tag; dabei wurden klinische Vitalparameter und laborchemische Parameter erfasst. Eine Blutabnahme erfolgte innerhalb von maximal 12 Stunden vor oder nach einer Messung. 109 PBR Messungen wurden insgesamt ausgewertet, in 106 Fällen davon fanden zugehörige Blutabnahmen statt. Die Messungen wurden je nach Gestationsalter bei Geburt in drei Gruppen gegliedert: sehr frühgeborene (Gruppe A [Gestationsalter bei Geburt < 30w + 0d]), moderat frühgeborene (Gruppe B [30w + 0d ≤ Gestationsalter bei Geburt < 37w + 0d]) und reifgeborene Neonaten (Kontrollgruppe [Gestationsalter bei Geburt ≥ 37w + 0d]). Für weitere Betrachtungen wurden die Messungen zum Zeitpunkt des Neugeborenen-Screenings als Annäherung für den PBR bei Geburt benutzt.

Ein signifikanter Anstieg der PBR (eine Reduktion der GCX) mit steigendem Gestationsalter wurde in allen drei Gruppen beobachtet. Der PBR der ersten Messung nach Geburt war zusätzlich signifikant abhängig vom Gestationsalter bei Geburt. Dieser Zusammenhang wurde bei allen gemessen frühreifen und reifen Neugeborenen durch die lineare Regressionsanalyse bestätigt. Weiterhin zeigte der PBR der Frühgeborenen im longitudinalen Verlauf eine Zunahme der PBR Größe, die wir als Gestationsalter-bedingten PBR Veränderungen deuteten. Diese ansteigenden Veränderungen des PBR waren in Gruppe A signifikant bis zu einem Gestationsalter von 32 Woche, ab dem sich ein beständiges Plateau zeigte, das weiterhin höhere PBR Werte als Gruppe B zwischen der 32. und 36. Gestationswoche präsentierte. Eine lineare Regressionsanalyse zeigte zusätzlich eine signifikante Abhängigkeit des PBR bezüglich des postnatalen Alters bei den ersten Messungen.

Folgender Zusammenhang zwischen PBR und Gestationsalter bei Geburt und im longitudinalen Verlauf wurde daraus abgeleitet: die anfällige, verletzliche perinatale GCX zeigt ein vermehrtes Shedding während einer extrauterinen Entwicklung im Vergleich zur physiologischen intrauterinen Reifung und präsentiert sich dadurch mit einer kleineren GCX (größeren PBR). Außer das Alter, wurden weitere Einflussgroßen getestet, aber kein Parameter, der einen signifikanten Unterschied zwischen der ersten und der letzten Messung zeigte, korrelierte bei der ersten und letzten Messung mit PBR. Das könnte an der kleinen Studienzahl liegen, da generell Korrelationen zwischen PBR und weiteren Parametern gefunden wurden, wenn alle Werte zusammen betrachtet wurden. Die Hauptbeschränkung dieser Studie waren die kleinen Gruppenzahlen, was sich auf die geringe Verfügbarkeit von stabilen, sehr frühgeborenen Neonaten und auf die entsprechenden geltenden Einschränkungen für Messungen zurückzuführen ist. Weiterhin ist zu erwähnen, dass PBR Messungen nur einen Rückschluss auf die GCX Größe, jedoch nicht auf die tatsächliche Funktionalität, zulassen.

Um die Ergebnisse dieser Studie zu bestätigen und zu verstärken, sind weitere Untersuchungen nötig, damit die Pathophysiologie bei Frühgeborenen besser verstanden werden kann.

7 References

1. Engele, J., *Herz-Kreislauf-System - Grundlagen*, in *Anatomie*, G. Aumüller, et al., Editors. 2014, Thieme Verlagsgruppe: Stuttgart, New York, Delhi, Rio.
2. Hornburger, M., *Endothelial hyperpermeability: characterization of novel drug targets and appropriate analytical methods.* 2013, LMU München: Fakultät für Chemie und Pharmazie
3. Baluk, P., et al., *Abnormalities of basement membrane on blood vessels and endothelial sprouts in tumors.* Am J Pathol, 2003. **163**(5): p. 1801-15.
4. Lowe, J.S., P.G. Anderson, and S.I. Anderson, *Stevens & Lowe's Human Histology-E-Book, Chapter 4*. 2018: Elsevier Health Sciences.
5. Krus, S., M.W. Turjman, and E. Flejka, *Comparative morphology of the hepatic and coronary artery walls. Part II. The relation between the internal elastic membrane, non-atherosclerotic intimal thickening and atherosclerosis.* Med Sci Monit, 2000. **6**(2): p. 249-52.
6. Silbernagl, S., A. Despopoulos jr, and A. Draguhn, *Austauschvorgänge am Endothel*, in *Taschenatlas Physiologie*, S. Silbernagl, A. Despopoulos jr, and A. Draguhn, Editors. 2018, Georg Thieme Verlag.
7. Rubenstein, D.A., W. Yin, and M.D. Frame, *Chapter 6 - Microvascular Beds*, in *Biofluid Mechanics (Second Edition)*. 2015, Academic Press: Boston. p. 227-266.
8. Lüllmann-Rauch, R., *11 Kreislauforgane*, in *Taschenlehrbuch Histologie*, R. Lüllmann-Rauch, Editor. 2015, Georg Thieme Verlag.
9. Gilbert, S.F., *Lateral Plate Mesoderm (Chapter 15) in Developmental biology*. 6. ed. 2000, Sunderland, Mass.: Sinauer. XVIII, 749 S. :.
10. Staub, N.C., *Pulmonary edema due to increased microvascular permeability to fluid and protein.* Circulation research, 1978. **43**(2): p. 143-151.
11. Herring, N. and D.J. Paterson, *Levick's Introduction to Cardiovascular Physiology*. 2018: CRC Press.
12. Kongstad, L., A.D. Moller, and P.O. Grande, *Reflection coefficient for albumin and capillary fluid permeability in cat calf muscle after traumatic injury.* Acta Physiol Scand, 1999. **165**(4): p. 369-77.
13. Chappell, D., et al., *Expedition glycocalyx.* Der Anaesthesist, 2008. **57**(10): p. 959-969.
14. Pries, A., *Physiologische Grundlagen der Mikrozirkulation: vaskuläre Adaptation.* Klinische Monatsblätter für Augenheilkunde, 2015. **232**(02): p. 127-132.
15. Pries, A.R. and T.W. Secomb, *Rheology of the microcirculation.* Clin Hemorheol Microcirc, 2003. **29**(3-4): p. 143-8.
16. Universitäten Fribourg, L.u.B.S.m.U.d.S.V.C. *Entwicklung der Gefässe: molekulare Grundlagen der Blutgefässentwicklung*. 2016 September 18, 2016 September 18, 2016]; Available from: http://www.embryology.ch/allemand/pcardio/gefassegrundlage01.html.
17. Käßmeyer, S., et al., *New Insights in Vascular Development: Vasculogenesis and Endothelial Progenitor Cells.* Anatomia, Histologia, Embryologia, 2009. **38**(1): p. 1-11.
18. Reitsma, S., et al., *The endothelial glycocalyx: composition, functions, and visualization.* Pflugers Arch, 2007. **454**(3): p. 345-59.
19. Cruz-Chu, E.R., et al., *Structure and response to flow of the glycocalyx layer.* Biophys J, 2014. **106**(1): p. 232-43.
20. Klitzman, B. and B.R. Duling, *Microvascular hematocrit and red cell flow in resting and contracting striated muscle.* American Journal of Physiology - Heart and Circulatory Physiology, 1979. **237**(4): p. H481-H490.
21. Pries, A., et al., *Resistance to blood flow in microvessels in vivo.* Circulation research, 1994. **75**(5): p. 904-915.
22. Desjardins, C. and B.R. Duling, *Heparinase treatment suggests a role for the endothelial cell glycocalyx in regulation of capillary hematocrit.* American Journal of Physiology-Heart and Circulatory Physiology, 1990. **258**(3): p. H647-H654.

23. Vink, H. and B.R. Duling, *Identification of distinct luminal domains for macromolecules, erythrocytes, and leukocytes within mammalian capillaries.* Circ Res, 1996. **79**(3): p. 581-9.
24. Luft, J.H., *Fine structures of capillary and endocapillary layer as revealed by ruthenium red.* Fed Proc, 1966. **25**(6): p. 1773-83.
25. van den Berg, B.M., H. Vink, and J.A. Spaan, *The endothelial glycocalyx protects against myocardial edema.* Circ Res, 2003. **92**(6): p. 592-4.
26. Hjalmarsson, C., B.R. Johansson, and B. Haraldsson, *Electron microscopic evaluation of the endothelial surface layer of glomerular capillaries.* Microvasc Res, 2004. **67**(1): p. 9-17.
27. Rostgaard, J. and K. Qvortrup, *Electron microscopic demonstrations of filamentous molecular sieve plugs in capillary fenestrae.* Microvasc Res, 1997. **53**(1): p. 1-13.
28. Nieuwdorp, M., et al., *Measuring endothelial glycocalyx dimensions in humans: a potential novel tool to monitor vascular vulnerability.* J Appl Physiol (1985), 2008. **104**(3): p. 845-52.
29. Goedhart, P., et al., *Sidestream Dark Field (SDF) imaging: a novel stroboscopic LED ring-based imaging modality for clinical assessment of the microcirculation.* Optics express, 2007. **15**(23): p. 15101-15114.
30. Lee, D.H., et al., *Deeper penetration of erythrocytes into the endothelial glycocalyx is associated with impaired microvascular perfusion.* PLoS One, 2014. **9**(5): p. e96477.
31. Barker, A.L., et al., *Observation and characterisation of the glycocalyx of viable human endothelial cells using confocal laser scanning microscopy.* Physical Chemistry Chemical Physics, 2004. **6**(5): p. 1006-1011.
32. Megens, R.T., et al., *Two-photon microscopy of vital murine elastic and muscular arteries. Combined structural and functional imaging with subcellular resolution.* J Vasc Res, 2007. **44**(2): p. 87-98.
33. Wilson, J. and T. Hunt, *Membrane structure (Chapter 10) in Molecular biology of the cell: the problems book*. 2014: Garland Science.
34. Lindahl, U. and M. Hook, *Glycosaminoglycans and their binding to biological macromolecules.* Annu Rev Biochem, 1978. **47**: p. 385-417.
35. Pries, A.R., T.W. Secomb, and P. Gaehtgens, *The endothelial surface layer.* Pflugers Arch, 2000. **440**(5): p. 653-66.
36. Weinbaum, S., J.M. Tarbell, and E.R. Damiano, *The structure and function of the endothelial glycocalyx layer.* Annu Rev Biomed Eng, 2007. **9**: p. 121-67.
37. Chaplin, M.F. and J.F. Kennedy, *Carbohydrate analysis: a practical approach.. ed. 2*. 1994: IRL Press Ltd.
38. Rao, L. and U. Pendurthi, *Tissue factor on cells.* Blood coagulation & fibrinolysis: an international journal in haemostasis and thrombosis, 1998. **9**: p. S27-35.
39. Muller, A.M., et al., *Comparative study of adhesion molecule expression in cultured human macro- and microvascular endothelial cells.* Exp Mol Pathol, 2002. **73**(3): p. 171-80.
40. Lipowsky, H.H., *Role of the Glycocalyx as a Barrier to Leukocyte-Endothelium Adhesion.* Adv Exp Med Biol, 2018. **1097**: p. 51-68.
41. Lawrence, M.B. and T.A. Springer, *Leukocytes roll on a selectin at physiologic flow rates: distinction from and prerequisite for adhesion through integrins.* Cell, 1991. **65**(5): p. 859-73.
42. Berndt, M.C., et al., *Purification and preliminary characterization of the glycoprotein Ib complex in the human platelet membrane.* Eur J Biochem, 1985. **151**(3): p. 637-49.
43. Hodivala-Dilke, K.M., A.R. Reynolds, and L.E. Reynolds, *Integrins in angiogenesis: multitalented molecules in a balancing act.* Cell Tissue Res, 2003. **314**(1): p. 131-44.
44. Corbel, C., *Expression of alphaVbeta3 integrin in the chick embryo aortic endothelium.* Int J Dev Biol, 2002. **46**(6): p. 827-30.
45. Ivetic, A., *A head-to-tail view of L-selectin and its impact on neutrophil behaviour.* Cell Tissue Res, 2018. **371**(3): p. 437-453.
46. Ley, K., *The role of selectins in inflammation and disease.* Trends Mol Med, 2003. **9**(6): p. 263-8.

47. Begandt, D., et al., *How neutrophils resist shear stress at blood vessel walls: molecular mechanisms, subcellular structures, and cell–cell interactions.* Journal of leukocyte biology, 2017. **102**(3): p. 699-709.
48. Goncharov, N.V., et al., *Markers and Biomarkers of Endothelium: When Something Is Rotten in the State.* Oxid Med Cell Longev, 2017. **2017**: p. 9759735.
49. Huang, M.T., et al., *Endothelial intercellular adhesion molecule (ICAM)-2 regulates angiogenesis.* Blood, 2005. **106**(5): p. 1636-43.
50. Schlesinger, M. and G. Bendas, *Vascular cell adhesion molecule-1 (VCAM-1)--an increasing insight into its role in tumorigenicity and metastasis.* Int J Cancer, 2015. **136**(11): p. 2504-14.
51. Davies, P.F., *Flow-mediated endothelial mechanotransduction.* Physiol Rev, 1995. **75**(3): p. 519-60.
52. Thi, M.M., et al., *The role of the glycocalyx in reorganization of the actin cytoskeleton under fluid shear stress: a "bumper-car" model.* Proc Natl Acad Sci U S A, 2004. **101**(47): p. 16483-8.
53. Nieuwdorp, M., et al., *Loss of endothelial glycocalyx during acute hyperglycemia coincides with endothelial dysfunction and coagulation activation in vivo.* Diabetes, 2006. **55**(2): p. 480-6.
54. Florian, J.A., et al., *Heparan sulfate proteoglycan is a mechanosensor on endothelial cells.* Circ Res, 2003. **93**(10): p. e136-42.
55. Mochizuki, S., et al., *Role of hyaluronic acid glycosaminoglycans in shear-induced endothelium-derived nitric oxide release.* Am J Physiol Heart Circ Physiol, 2003. **285**(2): p. H722-6.
56. Fung, Y.C. and S.Q. Liu, *Elementary Mechanics of the Endothelium of Blood Vessels.* Journal of Biomechanical Engineering, 1993. **115**(1): p. 1-12.
57. Rehm, M., et al., *Shedding of the endothelial glycocalyx in patients undergoing major vascular surgery with global and regional ischemia.* Circulation, 2007. **116**(17): p. 1896-906.
58. Mulivor, A.W. and H.H. Lipowsky, *Inflammation- and ischemia-induced shedding of venular glycocalyx.* Am J Physiol Heart Circ Physiol, 2004. **286**(5): p. H1672-80.
59. Grimm, J., R. Keller, and P.G. de Groot, *Laminar flow induces cell polarity and leads to rearrangement of proteoglycan metabolism in endothelial cells.* Thromb Haemost, 1988. **60**(3): p. 437-41.
60. Lipowsky, H.H. and A. Lescanic, *Inhibition of inflammation induced shedding of the endothelial glycocalyx with low molecular weight heparin.* Microvasc Res, 2017. **112**: p. 72-78.
61. Hu, X., et al., *Starling forces that oppose filtration after tissue oncotic pressure is increased.* Am J Physiol Heart Circ Physiol, 2000. **279**(4): p. H1724-36.
62. Levick, J.R., *Revision of the Starling principle: new views of tissue fluid balance.* J Physiol, 2004. **557**(Pt 3): p. 704.
63. Henry, C.B., W.N. Duran, and D.O. DeFouw, *Permselectivity of angiogenic microvessels following alteration of the endothelial fiber matrix by oligosaccharides.* Microvasc Res, 1997. **53**(2): p. 150-5.
64. Huxley, V.H. and F.E. Curry, *Albumin modulation of capillary permeability: test of an adsorption mechanism.* Am J Physiol, 1985. **248**(2 Pt 2): p. H264-73.
65. Kumase, F., et al., *Glycocalyx degradation in retinal and choroidal capillary endothelium in rats with diabetes and hypertension.* Acta Med Okayama, 2010. **64**(5): p. 277-83.
66. Nieuwdorp, M., et al., *Endothelial glycocalyx damage coincides with microalbuminuria in type 1 diabetes.* Diabetes, 2006. **55**(4): p. 1127-32.
67. Du, X.L., et al., *Hyperglycemia inhibits endothelial nitric oxide synthase activity by posttranslational modification at the Akt site.* J Clin Invest, 2001. **108**(9): p. 1341-8.
68. Algenstaedt, P., et al., *Microvascular alterations in diabetic mice correlate with level of hyperglycemia.* Diabetes, 2003. **52**(2): p. 542-9.
69. Ross , R., *Atherosclerosis — An Inflammatory Disease.* New England Journal of Medicine, 1999. **340**(2): p. 115-126.
70. Vink, H., A.A. Constantinescu, and J.A. Spaan, *Oxidized lipoproteins degrade the endothelial surface layer : implications for platelet-endothelial cell adhesion.* Circulation, 2000. **101**(13): p. 1500-2.

71. van den Berg, B.M., et al., *Atherogenic region and diet diminish glycocalyx dimension and increase intima-to-media ratios at murine carotid artery bifurcation.* Am J Physiol Heart Circ Physiol, 2006. **290**(2): p. H915-20.
72. Suematsu, M., et al., *The inflammatory aspect of the microcirculation in hypertension: oxidative stress, leukocytes/endothelial interaction, apoptosis.* Microcirculation, 2002. **9**(4): p. 259-276.
73. Henry, C.B. and B.R. Duling, *TNF-alpha increases entry of macromolecules into luminal endothelial cell glycocalyx.* Am J Physiol Heart Circ Physiol, 2000. **279**(6): p. H2815-23.
74. Zelova, H. and J. Hosek, *TNF-alpha signalling and inflammation: interactions between old acquaintances.* Inflamm Res, 2013. **62**(7): p. 641-51.
75. Becker, B.F., et al., *Degradation of the endothelial glycocalyx in clinical settings: searching for the sheddases.* Br J Clin Pharmacol, 2015. **80**(3): p. 389-402.
76. Nelson, A., et al., *Increased levels of glycosaminoglycans during septic shock: relation to mortality and the antibacterial actions of plasma.* Shock, 2008. **30**(6): p. 623-7.
77. Henderson-Toth, C.E., et al., *The glycocalyx is present as soon as blood flow is initiated and is required for normal vascular development.* Dev Biol, 2012. **369**(2): p. 330-9.
78. Allen, B.L., M.S. Filla, and A.C. Rapraeger, *Role of heparan sulfate as a tissue-specific regulator of FGF-4 and FGF receptor recognition.* J Cell Biol, 2001. **155**(5): p. 845-58.
79. Madri, J.A., J. Enciso, and E. Pinter, *Maternal diabetes: effects on embryonic vascular development--a vascular endothelial growth factor-A-mediated process.* Pediatr Dev Pathol, 2003. **6**(4): p. 334-41.
80. le Noble, F., et al., *Flow regulates arterial-venous differentiation in the chick embryo yolk sac.* Development, 2004. **131**(2): p. 361-75.
81. © Copyright World Health Organization (WHO). 2019 [cited 2019 18/07/2019]; Available from: https://www.who.int/news-room/fact-sheets/detail/preterm-birth.
82. Chawanpaiboon, S., et al., *Global, regional, and national estimates of levels of preterm birth in 2014: a systematic review and modelling analysis.* Lancet Glob Health, 2019. **7**(1): p. e37-e46.
83. Platt, M.J., *Outcomes in preterm infants.* Public Health, 2014. **128**(5): p. 399-403.
84. Saigal, S. and L.W. Doyle, *An overview of mortality and sequelae of preterm birth from infancy to adulthood.* Lancet, 2008. **371**(9608): p. 261-9.
85. Lee, H., et al., *In adolescence, extreme prematurity is associated with significant changes in the microvasculature, elevated blood pressure and increased carotid intima-media thickness.* Arch Dis Child, 2014. **99**(10): p. 907-11.
86. Puchwein-Schwepcke, A., et al., *Effects of Prematurity on the Cutaneous Microcirculatory Network in the First Weeks of Life.* Frontiers in Pediatrics, 2019. **7**(198).
87. Kerkhof, G.F., et al., *Does Preterm Birth Influence Cardiovascular Risk in Early Adulthood?* The Journal of Pediatrics, 2012. **161**(3): p. 390-396.e1.
88. Genzel-Boroviczeny, O., F. Christ, and V. Glas, *Blood transfusion increases functional capillary density in the skin of anemic preterm infants.* Pediatr Res, 2004. **56**(5): p. 751-5.
89. Weidlich, K., et al., *Changes in microcirculation as early markers for infection in preterm infants--an observational prospective study.* Pediatr Res, 2009. **66**(4): p. 461-5.
90. Echtler, K., et al., *Platelets contribute to postnatal occlusion of the ductus arteriosus.* Nat Med, 2010. **16**(1): p. 75-82.
91. Speer, C.P., *Neonatologie*, in *Pädiatrie*, C.P. Speer, M. Gahr, and J. Dötsch, Editors. 2019, Springer Berlin Heidelberg: Berlin, Heidelberg. p. 77-133.
92. Margraf, A., et al., *Maturation of Platelet Function During Murine Fetal Development In Vivo.* Arterioscler Thromb Vasc Biol, 2017. **37**(6): p. 1076-1086.
93. Hartnett, M.E. and J.S. Penn, *Mechanisms and management of retinopathy of prematurity.* N Engl J Med, 2012. **367**(26): p. 2515-26.
94. Mohamed, S., et al., *Hyperglycemia as a risk factor for the development of retinopathy of prematurity.* BMC Pediatr, 2013. **13**: p. 78.

95. van Teeffelen, D.J. and H. Vink, *Clinical assessment of vascular health with GlycoCheck™ Glycocalyx Measurement Software - A GlycoCheck™ Whitepaper*. 2012, GlycoCheck™ B.V., Oxfordlaan 70, 6229 EV Maastricht, The Netherlands: GlycoCheck™ B.V.
96. Groner, W., et al., *Orthogonal polarization spectral imaging: a new method for study of the microcirculation.* Nature medicine, 1999. **5**(10): p. 1209.
97. Medical, M. *MicroVision Medical*. 2014 17. Oktober 2018 um 16:48:46 MESZ [cited 2018 October]; Available from: http://www.microvisionmedical.com/.
98. Dane, M.J., et al., *Association of kidney function with changes in the endothelial surface layer.* Clin J Am Soc Nephrol, 2014. **9**(4): p. 698-704.
99. GraphPad Software, I. *GraphPad Statistics Guide*. 9. April 2018 [cited 2019; Available from: https://www.graphpad.com/guides/prism/7/statistics/index.htm?stat_how_to_correlation.htm.
100. The Endurance International Group, I. *PediTools Home* 2012 2019-01-12 [cited 2019; Available from: https://peditools.org/dates/.
101. Leistner, R., et al., *Nosocomial infections in very low birthweight infants in Germany: current data from the National Surveillance System NEO-KISS.* Klin Padiatr, 2013. **225**(2): p. 75-80.
102. Raaijmakers, A., et al., *Design and feasibility of "PREMATurity as predictor of children's Cardiovascular-renal Health" (PREMATCH): A pilot study.* Blood Press, 2015. **24**(5): p. 275-83.
103. Mercuro, G., et al., *Prematurity and low weight at birth as new conditions predisposing to an increased cardiovascular risk.* European Journal of Preventive Cardiology, 2013. **20**(2): p. 357-367.
104. Harfouche, R., et al., *Glycome and transcriptome regulation of vasculogenesis.* Circulation, 2009. **120**(19): p. 1883-1892.
105. Gorshkov, A.Y., et al., *Increase in perfused boundary region of endothelial glycocalyx is associated with higher prevalence of ischemic heart disease and lesions of microcirculation and vascular wall.* Microcirculation, 2018. **25**(4): p. e12454.
106. Gu, Y.M., et al., *Characteristics and determinants of the sublingual microcirculation in populations of different ethnicity.* Hypertension, 2015. **65**(5): p. 993-1001.
107. Uhl, B., *21.1 Allgemeines*, in *Gynäkologie und Geburtshilfe compact*, B. Uhl, Editor. 2013, Georg Thieme Verlag: Stuttgart.
108. Genzel-Boroviczeny, O., et al., *Orthogonal polarization spectral imaging (OPS): a novel method to measure the microcirculation in term and preterm infants transcutaneously.* Pediatr Res, 2002. **51**(3): p. 386-91.
109. Kroth, J., et al., *Functional vessel density in the first month of life in preterm neonates.* Pediatr Res, 2008. **64**(5): p. 567-71.
110. van Elteren, H., I.K. Reiss, and R.C. de Jonge, *Transcutaneous Microcirculatory Imaging in Preterm Neonates.* J Vis Exp, 2015(106): p. e53562.
111. Rassner, *2 - Aufbau und Aufgaben des Hautorgans*, in *Dermatologie (Neunte Ausgabe)*, Rassner, Editor. 2009, Urban & Fischer: Munich. p. 5-9.
112. Silbernagl, S., A. Despopoulos jr, and A. Draguhn, *Kreislaufregulation*, in *Taschenatlas Physiologie*, S. Silbernagl, A. Despopoulos jr, and A. Draguhn, Editors. 2018, Georg Thieme Verlag.
113. Cohen, B.A., *Kapitel 2 - Dermatologische Erkrankungen des Neugeborenen*, in *Pädiatrische Dermatologie (Zweite Ausgabe)*, B.A. Cohen and S. Tönjes, Editors. 2007, Urban & Fischer: Munich. p. 15-71.
114. Nussbaum, C., et al., *Perturbation of the microvascular glycocalyx and perfusion in infants after cardiopulmonary bypass.* The Journal of Thoracic and Cardiovascular Surgery, 2015. **150**(6): p. 1474-1481.e1.
115. De Backer, D., et al., *How to evaluate the microcirculation: report of a round table conference.* Critical Care, 2007. **11**(5): p. R101-R101.
116. Kudicke, C., *Bestimmung mikrozirkulatorischer Parameter bei gesunden Reifgeborenen in den ersten Lebenstagen*, in *Dissertation, LMU München: Medizinische Fakultät*. 2013.

117. Ergenekon, E., et al., *Peripheral microcirculation is affected during therapeutic hypothermia in newborns.* Arch Dis Child Fetal Neonatal Ed, 2013. **98**(2): p. F155-7.
118. van Elteren, H.A., et al., *Adaptation of the Cutaneous Microcirculation in Preterm Neonates.* Microcirculation, 2016. **23**(6): p. 468-74.
119. Kalia, Y.N., et al., *Development of skin barrier function in premature infants.* J Invest Dermatol, 1998. **111**(2): p. 320-6.
120. Weber, F., *Veränderung der Mikrozirkulation bei sehr unreifen Frühgeborenen in den ersten 48 Lebensstunden*. LMU München.
121. Haeren, R.H.L., et al., *In vivo assessment of the human cerebral microcirculation and its glycocalyx: A technical report.* Journal of Neuroscience Methods, 2018. **303**: p. 114-125.
122. Raaijmakers, A., et al., *Design and feasibility of "PREMATurity as predictor of children's Cardiovascular–renal Health" (PREMATCH): A pilot study.* Blood Pressure, 2015. **24**(5): p. 275-283.
123. Barker, D.J., *Fetal origins of coronary heart disease.* Bmj, 1995. **311**(6998): p. 171-4.
124. Mitchell, J.A. and B.R. Van Kainen, *Effects of alcohol on intrauterine oxygen tension in the rat.* Alcohol Clin Exp Res, 1992. **16**(2): p. 308-10.
125. Quine, D. and B.J. Stenson, *Arterial oxygen tension (Pao2) values in infants <29 weeks of gestation at currently targeted saturations.* Arch Dis Child Fetal Neonatal Ed, 2009. **94**(1): p. F51-3.
126. Jang, E.A., L.D. Longo, and R. Goyal, *Antenatal maternal hypoxia: criterion for fetal growth restriction in rodents.* Frontiers in Physiology, 2015. **6**(176).
127. Annecke, T., et al., *Shedding of the coronary endothelial glycocalyx: effects of hypoxia/reoxygenation vs ischaemia/reperfusion.* Br J Anaesth, 2011. **107**(5): p. 679-86.
128. Medlock, S., et al., *Prediction of Mortality in Very Premature Infants: A Systematic Review of Prediction Models.* PLOS ONE, 2011. **6**(9): p. e23441.
129. Suski, M., et al., *Prospective plasma proteome changes in preterm infants with different gestational ages.* Pediatr Res, 2018. **84**(1): p. 104-111.
130. Royland, J.E., G.W. Konat, and R.C. Wiggins, *Myelin gene activation: a glucose sensitive critical period in development.* J Neurosci Res, 1993. **36**(4): p. 399-404.
131. Franz, A.R., et al., *Intrauterine, Early Neonatal, and Postdischarge Growth and Neurodevelopmental Outcome at 5.4 Years in Extremely Preterm Infants After Intensive Neonatal Nutritional Support.* Pediatrics, 2009. **123**(1): p. e101-e109.
132. Belfort, M.B., et al., *Infant growth before and after term: effects on neurodevelopment in preterm infants.* Pediatrics, 2011. **128**(4): p. e899-906.
133. Ruys, C.A., et al., *Early-life growth of preterm infants and its impact on neurodevelopment.* Pediatric Research, 2018.
134. Cianfarani, S., D. Germani, and F. Branca, *Low birthweight and adult insulin resistance: the "catch-up growth" hypothesis.* Arch Dis Child Fetal Neonatal Ed, 1999. **81**(1): p. F71-3.
135. Ong, K.K., *Catch-up growth in small for gestational age babies: good or bad?* Current Opinion in Endocrinology, Diabetes and Obesity, 2007. **14**(1): p. 30-34.
136. Brandt, I., E.J. Sticker, and M.J. Lentze, *Catch-up growth of head circumference of very low birth weight, small for gestational age preterm infants and mental development to adulthood.* The Journal of Pediatrics, 2003. **142**(5): p. 463-470.
137. Alexeev, E.E., B. Lönnerdal, and I.J. Griffin, *Effects of postnatal growth restriction and subsequent catch-up growth on neurodevelopment and glucose homeostasis in rats.* BMC Physiology, 2015. **15**(1): p. 3.
138. Donati, A., et al., *Alteration of the sublingual microvascular glycocalyx in critically ill patients.* Microvascular Research, 2013. **90**: p. 86-89.
139. Nussbaum, C., et al., *Early microvascular changes with loss of the glycocalyx in children with type 1 diabetes.* J Pediatr, 2014. **164**(3): p. 584-9 e1.
140. Hales, C.N., et al., *Fishing in the Stream of Diabetes: From Measuring Insulin to the Control of Fetal Organogenesis.* Biochemical Society Transactions, 1996. **24**(2): p. 341-350.

141. Shane, A.L., P.J. Sánchez, and B.J. Stoll, *Neonatal sepsis.* The Lancet, 2017. **390**(10104): p. 1770-1780.
142. Jacobsen, B.B., et al., *Serum concentrations of thyroxine-binding globulin, prealbumin and albumin in healthy fullterm, small-for-gestational age and preterm newborn infants.* Acta Paediatr Scand, 1979. **68**(1): p. 49-55.
143. Martin, A., et al., *Preterm birth and oxidative stress: Effects of acute physical exercise and hypoxia physiological responses.* Redox Biology, 2018. **17**: p. 315-322.
144. Darland, D.C. and P.A. D'Amore, *Blood vessel maturation: vascular development comes of age.* J Clin Invest, 1999. **103**(2): p. 157-8.
145. Machin, D.R., et al., *Automated Measurement of Microvascular Function Reveals Dysfunction in Systemic Sclerosis: A Cross-sectional Study.* J Rheumatol, 2017. **44**(11): p. 1603-1611.
146. Christensen, R.D., et al., *The CBC: reference ranges for neonates.* Semin Perinatol, 2009. **33**(1): p. 3-11.
147. Jopling, J., et al., *Reference ranges for hematocrit and blood hemoglobin concentration during the neonatal period: data from a multihospital health care system.* Pediatrics, 2009. **123**(2): p. e333-7.
148. Muraca, M., et al., *Unconjugated and conjugated bilirubin pigments during perinatal development. II. Studies on serum of healthy newborns and of neonates with erythroblastosis fetalis.* Biol Neonate, 1990. **57**(1): p. 1-9.
149. Ullrich, D., et al., *The influence of gestational age on bilirubin conjugation in newborns.* Eur J Clin Invest, 1991. **21**(1): p. 83-9.
150. Berns, M. and C. Bührer, *Hyperbilirubinämie des Neugeborenen–Diagnostik und Therapie*, in *Leitlinien Kinder-und Jugendmedizin*. 2015, Elsevier. p. B7. 1-B7. 10.
151. Bachmaier, N. and C. Fusch, *8.2 Störungen im Säure-Basen-Gleichgewicht*, in *Neonatologie*, G. Jorch and A. Hübler, Editors. 2010, Georg Thieme Verlag: Stuttgart.
152. Top, A.P., et al., *Persistent low microcirculatory vessel density in nonsurvivors of sepsis in pediatric intensive care.* Crit Care Med, 2011. **39**(1): p. 8-13.
153. De Backer, D., et al., *Microvascular blood flow is altered in patients with sepsis.* Am J Respir Crit Care Med, 2002. **166**(1): p. 98-104.
154. Bonamy, A.K., et al., *Lower skin capillary density, normal endothelial function and higher blood pressure in children born preterm.* J Intern Med, 2007. **262**(6): p. 635-42.
155. Nathan, D.M., et al., *Intensive diabetes therapy and carotid intima-media thickness in type 1 diabetes mellitus.* N Engl J Med, 2003. **348**(23): p. 2294-303.

8 List of Charts

9 List of Figures

10 List of abbreviations

ANOVA	Analysis of variance
BE	Base excess
BPD	Bronchopulmonary dysplasia
CCD	Charge-coupled device
CD 44	Cluster of differentiation 44
CI	Confidence interval
CS	Chondroitine sulfate
d	Day(s)
DAPB	Dense peripheral actin band
DM	Diabetes melitus
D_{PERF}	Perfused diameter
E-selectin	Endothelial selectin
EC	Endothelial cell
EDRF	Endothelium-derived relaxing factor
EEC gap	Erythrocyte- endothelial- cell gap
Eq.	Equation
ESL	Endothelial surface layer
FGF	Fibroblast growth factor
FM	First measurement
GA	Gestational age (in weeks)
GAG	Glycosaminoglycans
Gal	Galactose
GCX	Glycocalyx
GlcUA	Glucuronic acid
GP	Glycoproteins
GPI	Glycophosphatidylinositol
HA	Hyaluronic acid
Hb	Hemoglobin (g/dl)
HCO_{3-}	Bicarbonate
Hct	Hematocrit (%)
HES	Hydroxyethyl starch
HR (in bpm)	Heart rate (in beats per minute)
HS	Heparane sulfate
ICAM	Intercellular adhesion molecule
IL	Interleukin
K	Fluid filtration coefficient ($m^3 \cdot s^{-1} \cdot mmHg^{-1}$)
K_a	Plasma reflection coefficient ($m^3 \cdot s^{-1} \cdot mmHg^{-1}$)
KS	Keratan sulfate
LDL	Low-density lipoprotein
LED	Light emitting diode
LM	Last measurement
LPS	Lipopolysaccharide
LSM	Laser scanning microscopy
MAP	Mean arterial pressure
mtp	Measurement time point
n	Amount
NEC	Necrotic enterocolitis
NICU	Neonatal intensive care unit
nm	Nanometer
NO	Nitric oxide
NS	Newborn screening
OPS-Imaging	Orthogonal polarized spectral imaging

Π	Osmotic pressure (mmHg)
P	Hydrostatic pressure (mmHg)
P-selectin	Platelet selectin
PBR	Perfused boundary region
pCO_2	Partial pressure of carbon dioxide (mmHg)
pdgf	Platelet-derived growth factor
PECAM	Platelet/endothelial cell adhesion molecule
PG	Proteoglycan
PN	Postnatal age
pO_2	Partial pressure of oxygen (mmHg)
Q_f	Net fluid flow ($m^3 \cdot s^{-1}$)
RBC	Red blood cell
ROP	Retinopathy of prematurity
ROS	Reactive oxygen species
RR	Respiratory rate
Δ	Difference
SD	Standard deviation
SDF	Sidestream Dark Field
SER	Serine
SOD	Superoxide dismutase
SpO_2	Oxygen saturation
TEM	Transmission electron microscopy
TNF-α	Tumor necrosis factor alpha
TPLSM	Two photon laser scanning microscopy
TVD	Total vascular density
VCAM	Vascular cell adhesion molecule 1
VEGF-a	Receptors for vascular endothelial growth factor
VVD	Valid vessel density
w	week(s)
WBC	White blood cell
Xyl	Xylose

11 Appendix (parents' consent)

Klinikum der Universität	München
Neonatologie im Perinatalzentrum Innenstadt Leitung: Prof. Dr. med. Orsolya Genzel-Boroviczény	Kinderklinik und Kinderpoliklinik im Dr. von Haunerschen Kinderspital Leitung: Prof. Dr. med. Dr. sci. nat. Christoph Klein

Information und Einverständniserklärung für die Studie:

„In vivo Untersuchung der mikrovaskulären Glykokalyx bei Neonaten und Kindern unter physiologischen Bedingungen und im Rahmen ausgewählter Pathologien."

Patienteninformation

Liebe Eltern, liebe Erziehungsberechtigte,

Wie Sie bereits im Gespräch mit uns erfahren haben, führen wir eine Studie mit dem Titel „In-vivo Untersuchung der mikrovaskulären Glykokalyx bei Neonaten und Kindern unter physiologischen Bedingungen und im Rahmen ausgewählter Pathologien" durch.
In dieser Studie geht es darum, neue Erkenntnisse über den Aufbau und die Funktion der kleinsten Blutgefäßen zu erlangen. Ziel ist es die Entstehung von Erkrankungen, welche mit einer Fehlregulation der Gefäße und Durchblutungsstörungen einhergehen, besser zu verstehen, um diese besser behandeln zu können. Zu solchen Erkrankungen zählen bespielsweise schwere Infektionen und akute Veränderungen der Blutzusammensetzung aber auch chronische Erkrankungen wie Diabetes mellitus oder angeborene Herzfehler.
Von besonderem Interesse ist hierbei eine Struktur der Gefäßwand, die sich Glykokalyx nennt. Hierbei handelt es sich um eine Schicht aus Zucker- und Eiweißbestandteilen, welche jedes gesunde Gefäß von innen ausgekleidet. Untersuchungen an Erwachsenen haben gezeigt, dass die Glykokalyx eine zentrale Rolle bei der Regulation der Gefäßfunktionen einnimmt. Ein Abbau oder Veränderung der Zusammensetzung der Glykokalyx können daher zu Fehlfunktion der Blutgefäße führen. Die Folgen sind vielfältig und reichen bis zum Organversagen. Bei Kindern ist bislang unklar wie weit die Glykokalyx bereits ausgebildet ist und ob eine Schädigung zur Entstehung von Komplikationen im Rahmen der o.g. Erkrankungen führt.

Wir möchten daher mittels einer kleinen Kamera die Gefäße Ihres Kindes direkt untersuchen. Hierzu legen wir je nach Alter des Kindes einen kleinen Messfühler an die Ohrmuschel, den Oberarm oder unter die Zunge. Dieser entsendet grünes Licht ins Gewebe, welches von den roten Blutkörperchen in den Gefäßen absorbiert wird, während das umliegende Gewebe das Licht reflektiert. Hierdurch können wir die Gefäße darstellen und mit einer Videokamera aufzeichnen. Die Lichtquelle ist so konzipiert, dass es zu keiner Erwärmung oder anderen Auswirkungen auf die Haut kommt. Die Messung dauert ca. 15

Minuten und ist für Ihr Kind vollkommen schmerzlos und ohne Risiko. Sie können selbstverständlich gerne bei der Untersuchung anwesend sein.

Um zu klären, welche Faktoren möglicherweise zu einem Abbau der Glykokalyx führen, möchten wir zudem bestimmte Blutwerte (z.B. Blutzucker, Hämoglobinwert) bestimmen. Hierfür versuchen wir die Messungen zu einem Zeitpunkt durchzuführen, an welchem eine klinisch notwendige Blutentnahme vorgesehen ist, damit ihr Kind keiner zusätzlichen Blutentnahme ausgesetzt wird. Wir werden dann im Rahmen dieser Blutentnahme etwa 5-10 ml Blut (bei Säuglingen 2 ml) gewinnen. Falls dies nicht möglich ist, verzichten wir auf eine Blutentnahme aus einer Vene und würden dafür ggf. nur einen kleinen Fingerpiks machen. Weiterhin kann es notwendig sei, dass wir eine Urinprobe von ihrem Kind nehmen oder sogar eine Urinsammlung über 24-Stunden veranlassen, um die Abbauprodukte der Glykokalyx im Urin zu messen. Diese Untersuchungen sollen helfen die Mechanismen, welche zu einer Schädigung der Glykokalyx führen aufzuklären.

Sie können vollkommen frei entscheiden, ob Sie einer Teilnahem ihres Kindes an der Studie zustimmen. Sollten Sie ablehnen, wird dadurch keinerlei Nachteil für die weitere medizinische Versorgung Ihres Kindes entstehen. Sie können Ihr Einverständnis jederzeit ohne Angabe von Gründen zurückziehen. Im Falle eines Rücktritts von der Studie wird bereits gewonnenes Material vernichtet, es sei denn, Sie erklären sich trotz des Rücktritts von der Studie mit der Auswertung des Materials bzw. der Daten bereit. In diesem Fall wird das Material nur in irreversibel anonymisierter Form weiter verwendet.

Datenschutz:

Nur direkt mit der Studie betraute Personen haben im Rahmen der entsprechenden gesetzlichen Vorschriften Zugang zu den vertraulichen Daten, in denen die Probanden namentlich genannt werden. Diese Personen unterliegen der Schweigepflicht und sind zur Beachtung des Datenschutzes verpflichtet. Dritte erhalten keinen Einblick in Originalkrankenunterlagen. Für die Interpretation der Untersuchungsergebnisse ist es u.U. notwendig, dass nachträglich eine Zuordnung der Messungen oder Proben zu den Probanden erfolgt, um beispielsweise eine Korrelation mit klinischen und laborchemischen Daten vornehmen zu können, welche zum Messzeitpunkt noch nicht vorlagen. Um dies zu gewährleisten, werden die Daten pseudomnymisiert. Hierzu erhält jedes Kind eine fortlaufende Studiennummer (001, 002, 003 usw.), welche weder Initialen noch Geburtsdatum oder sonstige personenbezogene Merkmale enthält. Alle Messungen und Proben eines Probanden werden unter dieser Studiennummer geführt. Die Weitergabe der Daten erfolgt ausschließlich zu statistischen und wissenschaftlichen Zwecken ohne namentliche Nennung. Auch in etwaigen Veröffentlichungen der Daten dieser Studie findet keine namentliche Nennung statt. Die Daten werden in der Abteilung für Neonatologie der Kinderklinik im Perinatalzentrum Innenstadt zehn Jahre lang aufbewahrt

Gerne können Sie sich bei weiteren Fragen an einen der verantwortlichen Ärzte wenden.

Wir würden uns sehr freuen, wenn Sie der Teilnahme Ihres Kindes zustimmen würden. Sie helfen damit den jungen Patienten.

Mit freundlichen Grüßen

Dr. med. Claudia Nußbaum
Assistenzärtzin für Kinderheilkunde

Dr. med. Alexandra Puchwein-Schwepcke
Assistenzärztin für Kinderheilkunde

Einverständniserklärung

Hiermit erkläre ich mich mit der Teilnahme meines Kindes ……
an der Studie „In vivo Untersuchung der mikrovaskulären Glykokalyx bei Neonaten und Kindern unter physiologischen Bedingungen und im Rahmen ausgewählter Pathologien“ einverstanden.

Ich wurde darüber aufgeklärt, dass die im Rahmen der Studie gewonnenen Proben und Daten in verschlüsselter Form gespeichert und ausgewertet werden. Für die Verschlüsselung werden die Proben mit fortlaufenden Nummern versehen, ohne jeglichen Hinweis auf die Person wie Geburtsdatum oder Initialen. Ich bin mit der Weitergabe der Daten in verschlüsselter Form ausschließlich zu statistischen und wissenschaftlichen Zwecken im Rahmen der Studie einverstanden.

Ich wurde darauf hingewiesen, dass die Teilnahme an dieser Studie freiwillig ist und aus einer Nichtteilnahme meinem Kind keinerlei Nachteile entstehen. Ich bin darüber informiert, dass ich jederzeit und ohne Angabe von Gründen meine Einwilligung zur Teilnahme an der Studie widerrufen kann.

Die Studie wurde mir von …….. in einem persönlichen Gespräch ausführlich und verständlich erklärt und ich habe keine weiteren Fragen bezüglich der Durchführung dieser Untersuchungen. Ich hatte ausreichend Zeit mich zu entscheiden.

Ort, Datum Name und Unterschrift mind. eines Elternteils/Erziehungsberechtigen

---

Ort, Datum Name und Unterschrift des Arztes

Ich bin einverstanden, dass im Rahmen der Untersuchung aufgezeichnete Daten in verschlüsselter Form gespeichert und ausgewertet werden. Mir wurde zugesichert, dass personenbezogene Daten stets absolut vertraulich behandelt werden und nicht in die Öffentlichkeit gelangen.

Ort, Datum Name und Unterschrift mind. eines Elternteils/Erziehungsberechtigen

---

Ort, Datum Name und Unterschrift des Arztes

12 Danksagung

Ich bedanke mich bei allen, die diese Arbeit durch ihre ständige Unterstützung möglich gemacht haben. Inhaltlich und fachlich bin ich PD. Dr. med. Claudia Nußbaum für ihre permanente Hilfe und Korrektur dankbar, genauso sehr danke ich meiner Doktormutter Frau Prof. Genzel-Boroviczeny, die mir diese Arbeit ermöglicht hat.

Für die persönliche Unterstützung habe ich allen voran meiner Familie und meinen Liebsten zu danken, die diese lange Zeit stets für mich da war und die immer unterstützt und motiviert haben. Danke für die ständige Unterstützung.

13 Affidavit/ Eidesstaatliche Erklärung

Hiermit erkläre ich, dass ich die vorliegende Arbeit eigenständig und ohne fremde Hilfe angefertigt habe.

Textpassagen, die wörtlich oder dem Sinn nach auf Publikationen oder Vorträgen anderer Autoren beruhen, sind als solche kenntlich gemacht. Die Arbeit wurde bisher keiner anderen Prüfungsbehörde vorgelegt und auch noch nicht veröffentlicht.

Berlin, 18.04.2021	Lea Rajwich
Ort, Datum	Unterschrift